Palaeogeography, Palaeoclimatology, Palaeoecology 674 (2025) 113039

Contents lists available at ScienceDirect

Palaeogeography, Palaeoclimatology, Palaeoecology

journal homepage: www.elsevier.com/locate/palaeo

Onset of large-scale terrestrial organic carbon burial driven by Early Devonian changes in vascular plants and environments

Lusheng Yin [a], Minfang Yang [b], Jing Lu [a,*], Ziyu Ling [a], Xiaoyu Hu [a], Xiao Bian [a], Kai Zhou [a], Peixin Zhang [c], Le Liu [a], Longyi Shao [a], Jason Hilton [d,*], David P.G. Bond [e,*]

[a] State Key Laboratory for Fine Exploration and Intelligent Development of Coal Resources, College of Geoscience and Surveying Engineering, China University of Mining and Technology, Beijing 100083, PR China
[b] Research Institute of Petroleum Exploration and Development, Petro China, Beijing 100083, PR China
[c] School of Municipal and Environmental Engineering, Henan University of Urban Construction, Pingdingshan, Henan 467036, PR China
[d] School of Geography, Earth and Environmental Sciences, The University of Birmingham, Edgbaston, Birmingham B15 2TT, UK
[e] School of Environmental Sciences, University of Hull, Hull HU6 7RX, UK

ARTICLE INFO

Editor: H Falcon-Lang

Keywords:
South China
Facies association
Plant terrestrialization
Total Organic Carbon (TOC)
Kerogen macerals
Plant geoengineers

ABSTRACT

The Early Devonian witnessed a major phase in the terrestrialization of land by plants. Understanding the implications for organic matter formation and accumulation during this interval is key to understanding global carbon burial. Existing research on the Early Devonian primarily focuses on marine carbonate records that do not permit evaluation of the mechanisms of terrestrial organic carbon burial, particularly in the early stages of plant colonization. Here, we examine facies associations, environmental evolution, and organic carbon burial within the late Pragian aged Posongchong Formation at the Zhichang section in Wenshan, Yunnan Province, China, a formation previously noted for recording the early radiation of land plants in coastal settings. Sedimentological and geochemical data include: (1) Paleosalinity proxies (B* and B/Ga) and sedimentary structures that indicate fluviolacustrine Facies Association (FA A), tidal flat (FA B), and shallow marine (FA C) facies developed in the study area, with two pulses of deepening separated by shallowing; (2) Total Organic Carbon (TOC) and kerogen maceral analyses that reveal an increase in terrestrial organic carbon content derived from terrestrial higher plants and phytoplankton; and (3) Organic matter preserved in coaly and carbonaceous shales that is mainly derived from continental higher plants that grew in a restricted, stable freshwater-brackish lagoon and floodplain environment. The land plant radiation recorded by the Posongchong Formation occurred within a stable coastal plain that provided a suitable setting for the supply and preservation of organic carbon in this early terrestrial ecosystem, in turn influencing the development of global terrestrial carbon burial.

1. Introduction

The Early Devonian is a key interval in geological history that witnessed significant changes in climate, ocean chemistry, and sea levels (e.g., Saltzman, 2002; Buggisch and Mann, 2004; Buggisch and Joachimski, 2006; Joachimski et al., 2009; Bábek et al., 2018a, 2018b; Slavík and Hladil, 2020; Weinerová et al., 2020). During this time, the terrestrial landscape was colonized by vascular plants (e.g., Algeo and Scheckler, 1998; Gensel and Edwards, 2001; Cascales-Miñana et al., 2017), a process that, along with changing paleogeographies (e.g., Wu et al., 1997), had a profound impact on global biogeochemical cycles (e.g., Małkowski and Racki, 2009; Lenton et al., 2012, 2018; Husson et al., 2016; Xue et al., 2016; Chen et al., 2021). Recently, increasing attention has been paid to the relationship between global environmental changes and biological events during the Early Devonian (e.g., Slavík and Hladil, 2020; Chen et al., 2021; Frýda et al., 2021). However, most of these studies have focused on marine carbonate records from North America, Europe, and Australia (e.g., Saltzman, 2002; Buggisch and Joachimski, 2006; Buggisch et al., 2008; Weinerová et al., 2020), while contemporaneous data from China remain limited, especially those on organic matter accumulation and burial in clastic and terrestrial sedimentary systems.

The enrichment of organic matter in sediments is a complex and nonlinear geological process, influenced by the interaction of multiple

* Corresponding authors.
E-mail addresses: lujing@cumtb.edu.cn (J. Lu), j.m.hilton@bham.ac.uk (J. Hilton), d.bond@hull.ac.uk (D.P.G. Bond).

https://doi.org/10.1016/j.palaeo.2025.113039
Received 10 April 2025; Received in revised form 15 May 2025; Accepted 15 May 2025
Available online 20 May 2025

factors such as paleosalinity, primary productivity and terrigenous input (Carroll and Bohacs, 1999; Sageman et al., 2003; Zhang et al., 2018). Some studies of the Early Devonian suggest that the colonization of terrestrial landscapes by vascular plants played a crucial role in organic carbon burial (Algeo and Scheckler, 1998; Algeo et al., 2001). For example, Chen et al. (2021) argued that the physiological activities of vascular plants increased the rate and intensity of continental weathering (Sandberg et al., 1988; Algeo and Scheckler, 1998; Algeo et al., 2001). Terrestrialization by plants is also implicated in marine anoxia and black shale development through changing surface runoff and element cycling in the terrestrial environment (Algeo and Scheckler, 1998; Xue et al., 2022, 2023a, 2023b), thereby accelerating organic carbon burial in sediments (Joachimski et al., 2002; Joachimski and Buggisch, 2002; Morris et al., 2015). However, recent studies suggest that the development of early vascular plants was related to the transformation of river or coastal landform and morphology, e.g. by increasing river landscape stability and driving the extensive development of meandering rivers, and creating soils with roots (Davies and Gibling, 2010; Gibling and Davies, 2012; McMahon and Davies, 2018). These changes in terrestrial environments stimulated the accumulation of organic matter (Xue et al., 2016, 2022).

The Lower Devonian Posongchong Formation, exposed in the Wenshan area of Yunnan Province, represents a typical transitional facies sequence from the Early Devonian of South China. It preserves a rich fossil record, a comprehensive sedimentary history, a diverse range of sedimentary environments, and a relatively stable geological structure (see Hao and Xue, 2013 for summary), making it an ideal location for studying sedimentary evolution during the Early Devonian. Additionally, the Early Devonian was a significant period of radiation among vascular plants (Bateman et al., 1998; Gensel and Edwards, 2001; Gerienne et al., 2016; Cascales-Miñana et al., 2017; Xue et al., 2018, 2023a, 2023b), and the evolution of plant life during this time is crucial for understanding changes in climate, sedimentary environments, and carbon burial (e.g., Algeo et al., 2001; Xue et al., 2022). The relationship between regional sedimentary events and global or regional climate and environmental changes in the Early Devonian is not well understood – hence the motivation for this study. Here, we examine transitional facies sediments from the Zhichang section, located in the Wenshan area of the South China Plate. We utilize outcrop sequences, sedimentary structures, bioturbation features, and paleosalinity indexes to identify facies associations and sea level changes, and to explore the sedimentary controls on the preservation and burial of organic carbon in Earth's Early

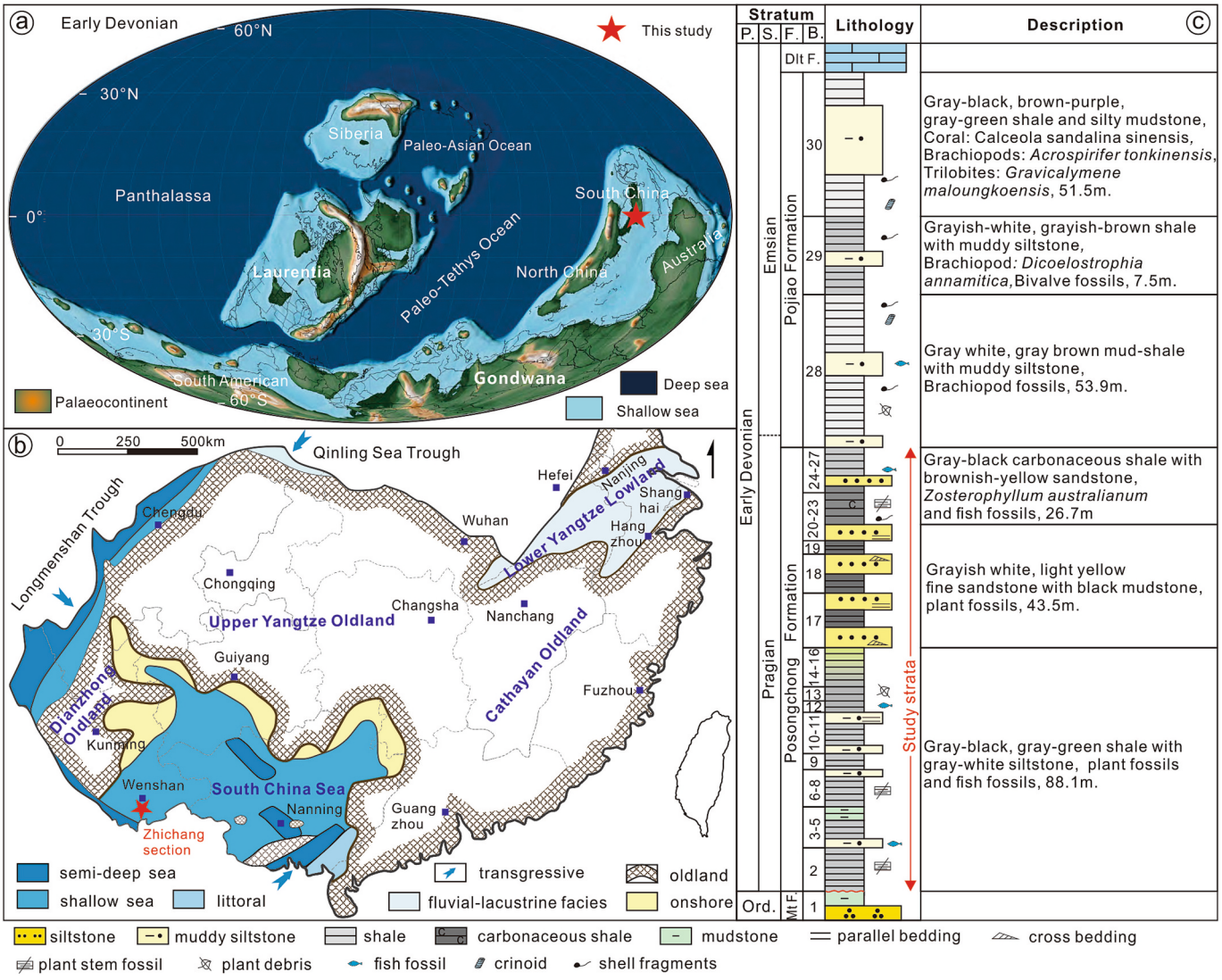

Fig. 1. Location and geological context for the study area including (a) Early Devonian paleogeographic map (Scotese, 2014) showing the position of the South China; (b) Paleogeographic map of the South China during deposition of the Posongchong Formation showing the position of the Wenshan (modified form Shu et al., 2021); (c) Stratigraphic distributions of plant megafossil and biozones (modified from Xue et al., 2018;). Abbreviations: P = Period; Ord. = Ordovician; S. = Stage; F. =Formation; B. = Bed; Dlt = Daliantang; Mt. = Meitan.

Devonian surficial environments.

2. Geological setting

The South China Plate is located along the eastern margin of the Paleo-Tethys Ocean and is composed of the Yangtze Block, Cathaysia Block and Jiangnan Orogenic Belt (e.g., Shu et al., 2021; Fig. 1a, b). The Qinling-Dabie-Sulu Orogenic belt is separated from the North China Plate to the north. The Longmenshan-Hengduanshan fault is connected with the Tibetan Plateau to the west, and the Southeast Asian Block is in contact with the Changning-Majang fault to the southwest. The West Pacific tectonic region lies to the southeast (Shu et al., 2021; Fig. 1b). The studied section records deposition in a low paleolatitude area of the southern South China Plate (Fig. 1a). During the Caledonian orogeny, in the Silurian, this area experienced widespread uplift and denudation, leading to an angular unconformity between Devonian sequences and underlying strata (Wang et al., 2024). The basement consists of Proterozoic metamorphic rocks (gneiss, quartzite, schist), and the sediment for the Devonian sediments is mainly sourced from the Vietnam Oldland as well as the Ailaoshan metamorphic series (Burrett et al., 2014; Lai et al., 2014; Xia et al., 2016). Large-scale transgression during the Pragian (Early Devonian) led to significant changes in paleogeography and paleoenvironments. A narrow bay formed between the Vietnam Oldland and the Maguan Oldland, creating a coastal plain and shallow marine environment (Wu, 2001; Liao and Ruan, 2003; Rong et al., 2003; Hao and Xue, 2013; Fig. 1b).

The Zhichang section, located southeast of Wenshan in Yunnan Province, serves as the standard section of the Lower Devonian in southern Yunnan and is well exposed (Fig. 1b, c). The stratigraphic sequence, from oldest to youngest, includes the Lower-Middle Ordovician Meitan Formation, the Lower Devonian Posongchong, Pojiao, and Daliantang Formations, the Middle-Upper Devonian Pozheluo, Liujiang, and Wuzhishan Formation (Jin et al., 2005; Hao and Xue, 2013; Qie et al., 2019a, 2021a, 2021b; Wang et al., 2024). Jin et al. (2005) divided the Posongchong Formation into 3 beds, and these were later refined into 9 beds by Hao and Xue (2013). Our detailed study divides this strata into 26 beds (C2-C27) from bottom to top, with bed C1 marking the top of the underlying Meitan Formation. The contact between the quartz sandstone of the Meitan Formation and the Posongchong Formation is unconformable, while the Posongchong / Pojiao contact appears conformable (Jin et al., 2005; Hao and Xue, 2013). The age of the Posongchong Formation is constrained by the marine faunas of the overlying Pojiao Formation, including the late Pragian-early Emsian brachiopod assemblages (*Euryspirifer-Dicoelostrophia*), corals (*Xystriphylloides nobilis*) and *Siphonophrentis angusta* fauna, all of which indicate a late Pragian (or latest) Pragian to earliest Emsian age for the Pojiao Formation (Jin et al., 2005; Hao and Xue, 2013; Lu and Chen, 2016). Additionally, the Posongchong Formation is associated with the spore assemblages *Apiculiretusispora plicata - Dibolisporites emsiensis* (PE), *Verrucosporites polygonalis* (Wang, 1994), which correlate with the Pragian of the Old Red Sandstone Continent (Streel, 1967; Streel et al., 1987; Richardson and McGregor, 1986; Steemans, 1989). Wang (1994) placed the Posongchong Formation within the PE (*polygonalus-emsiensis*) spore assemblage zone, just below the AS (*annulatus-sextantii*) zone of Richardson and McGregor (1986), further supporting a late Pragian age (Cascales-Miñana et al., 2017). This conclusion is corroborated by the associated fish fossil assemblages (Fang et al., 1994; Zhu et al., 1994).

3. Material and methods

For this study, fresh samples were collected from exposed strata of the Lower Devonian Posongchong Formation at the Zhichang section in Wenshan. The target strata were re-logged and sampled with high precision following earlier work by Jin et al. (2005) and Hao and Xue (2013), who divided the Posongchong Formation into 3 beds and 9 beds respectively. Through detailed lithological analysis we divided the Posongchong Formation into 26 beds (C2-C27) from bottom to top (bed C1 marks the top of the underlying Meitan Formation). Lithologies, bed numbers and thicknesses, as well as physical and biogenic sedimentary structures were documented, along with the characteristics of bed contacts, textures, fabrics, and colors. Additional notable features, such as ferruginous nodules, rootlets, and carbonaceous debris, were also recorded. A subset of these fresh samples was selected for further geochemical and petrological analysis.

A total of 43 mudstone samples were collected from the Posongchong Formation at Zhichang and were divided into two parts. One part was crushed into particles of 1 mm diameter for kerogen enrichment. The remaining samples were pulverized into a powder with diameters of about 200-mesh and divided into 4 parts, and analyzed for major elements, trace elements, total organic carbon and total sulfur at the State Key Laboratory for Fine Exploration and Intelligent Development of Coal Resources. The total sulfur (TS) analysis was carried out using an Eltra carbon-sulfur analyzer (Eltra CS-i), according to the Chinese National Standard (GB/T19145–2003), with a detection limit of 30 μg/g and absolute analysis error of ±5 %. Major elements analysis was carried out using an X-ray fluorescence spectrometer (PW2404). The spectrometer was calibrated before use with standards of CRMs (GBW7427), and analytic precision was within 5 %. Trace elements analysis was undertaken with an iCAP-Q inductively coupled plasma mass spectrometer (ICP-MS) and Milestone Ethos UP microwave digestion instrument, according to China national standard (GB/T 14506.29–2010, GB/T 14506.30–2010), with analytic precision within 5 %. In situ preparation of polished section and rock thin section and identification of microscopic composition were completed in the State Key Laboratory for Fine Exploration and Intelligent Development of Coal Resources, in accordance with the Chinese National standard (SY/T5368–2003; SY/T5368–2016). Kerogen enrichment and identifications were conducted at the Research Institute of Petroleum Exploration and Development of China according to the Chinese National standard (SY/ T5125–2014), with no less than 300 effective points per sample analyzed. The mineral types were identified under a microscope (LEICA DM4500P LED), according to the principles of Syvitski (1991). Grain-size analysis of clastic rock samples was performed using an image analyzer that determined the edges of individual particles.

The lithofacies of the outcrops in the study area are classified based on sedimentary characteristics, following the method proposed by Fielding et al. (2022) for lithofacies characteristics and facies associations. The key characteristics of the lithofacies defined in this study (such as lithology, thickness, physical and biogenic sedimentary structures, and other features) are summarized in Supplementary Table 2 and Fig. 2. The Bioturbation Index (BI) was used to quantify the sedimentary structural changes induced by biological activities and the degree of bioturbation (Taylor and Goldring, 1993), enabling the reconstruction of paleo-ecological conditions and the paleoenvironmental state at the time of deposition. The paleosalinity index, determined through geochemical analysis, was used for quantitative analysis of paleosalinity, which further supports the interpretation of sedimentary facies. Fluviolacustrine, tidal flat, shallow marine and other coastal terms (coastal plain, shoreface, offshore shelf) and hydrographical datums (Extreme High Water Level, Mean High Water Level, Mean Low Water Level) are based on “Graphic Definition of Coastal Terms” (Finkl and Makowski, 2019) and “Coastal Geology” (Morales, 2022).

Water salinity is a critical factor in determining sedimentary environments under a humid climate, influencing the transition from continental to transitional and marine facies. Typically, water salinity changes from freshwater to brackish and then to saltwater, seawards. Boron (B) is enriched in marine argillaceous sediments, where it is adsorbed onto clay minerals by substituting H_2O and OH^- ions on the surface of α–Al_2O_3 (Keren and Mezuman, 1981). Higher pH and lower temperatures generally enhance the adsorption affinity of clay minerals for B. Notably, boron can substitute for silicon and aluminum in the tetrahedral coordination of the muscovite structure within the illite

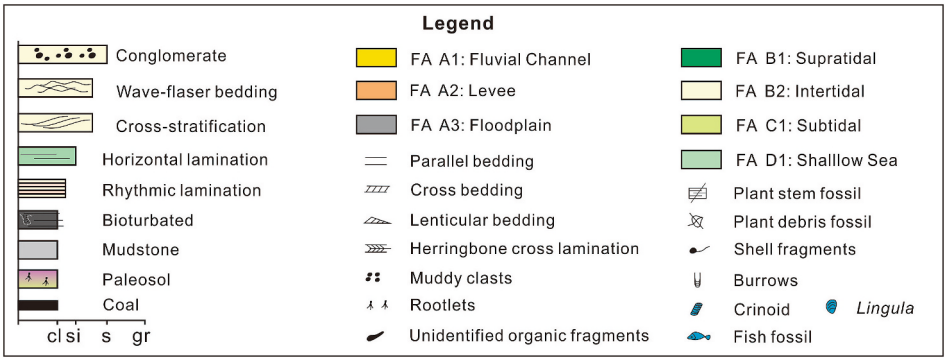

Fig. 2. Facies Association legend.

lattice (Harder, 1970). Therefore, the B content of illite (with illite content >70 %) is considered a reliable proxy for paleosalinity. If the rock contains other mineral impurities, the theoretical potassium content of 8.5 % in illite can be used to convert the boron content into that of pure illite, a process known as corrected boron content (B*), which is calculated using the formula: ($B^* = B \times 8.5 / \%K_2O$) (e.g., Walker and Price, 1963, Walker, 1968; Ye et al., 2016). The corrected boron content ranges from 300 to 400 ppm in normal marine environments, 200–300 ppm in brackish environments, and less than 200 ppm in freshwater environments (Ye et al., 2016). Gallium (Ga) is abundant in freshwater sediments and is predominantly concentrated in aluminum-containing minerals, such as clay minerals. Since Ga^{3+} replaces structural sites typically occupied by Al^{3+}, its migration and precipitation are primarily controlled by the chemical properties of aluminum (e.g., Hawkins and Roy, 1963; Wang et al., 2011; Breiter et al., 2013). During diagenesis, Ga remains a relatively immobile element, incorporated into the structures of resistant minerals (Panahi et al., 2000). Under alkaline pore water conditions, Ga adsorbed onto clay minerals tends to be immobile. Due to the differing behaviors of B and Ga in sedimentary entrainment processes, the ratio of B/Ga has been effectively used to indicate the paleosalinity of water bodies and to distinguish between marine and terrestrial facies (Potter et al., 1963; Chen et al., 1997; Yuri et al., 2008). However, controlled by sediment type and provenance differences, the B/Ga ratio thresholds for salinity in various water bodies can vary across different regions and time periods (e.g., Wang et al., 1979; Qian and Shi, 1982; Wei and Algeo, 2020). Based on the established B/Ga ratio boundaries for freshwater, brackish water, and seawater, and incorporating sedimentary and fossil evidence from the study area, we determined that the B/Ga ratio boundaries for the Early Devonian in the study area are as follows: freshwater (<3), brackish water (3–6), and seawater (>6) (Wei and Algeo, 2020; Fig. S1).

4. Results and analysis

4.1. Paleosalinity

The concentrations / values of B, Ga, B*, and B/Ga are shown in Supplementary Table 1. The B values vary from 53.75 to 116.54 μg/g ($\bar{x}$ = 91.22 μg/g), while B* values vary from 118.96 to 412.64 μg/g ($\bar{x}$ = 217.89 μg/g). The Ga the B* values vary from 10.15 to 27.50 μg/g ($\bar{x}$ = 18.55 μg/g), and B/Ga ratios vary from 2.23 to 9.38 μg/g ($\bar{x}$ = 5.16 μg/g).

The B value in beds C2, C3, C12, and C13 are relatively high, varying from 101.26 to 116.54 μg/g ($\bar{x}$ = 108.37 μg/g), while Ga values vary from 12.09 to 27.50 μg/g ($\bar{x}$ = 22.31 μg/g). The vertical trends of B and Ga values are similar, indicating that the two elements are likely to share similar occurrence states, and the B/Ga ratio can be used as proxy for paleosalinity changes (correlation coefficient r = +0.358, n = 39). The trend of B* values is consistent with that of the B/Ga ratio, demonstrating a strong correlation between the two as a result of paleosalinity changes (correlation coefficient r = +0.728, n = 39). High TOC values are observed in beds C2-C3 ($\bar{x}$ = 0.79 %), C12-C13 ($\bar{x}$ = 0.66 %), C18 ($\bar{x}$ = 0.68 %) and C24-C26 ($\bar{x}$ = 1.99 %), which align with Ga values at those levels (correlation index r = +0.678, n = 39). In contrast, the TOC values show an inverse relationship with the B/Ga ratio (correlation coefficient r = −0.424, n = 39), suggesting that higher levels of TOC accumulated in freshwater sedimentary environments, with a strong affinity for clay minerals (Fig. S2).

Based on the above analysis, the environmental conditions indicated by the B/Ga ratio and B* values are consistent with the sedimentary background of the Posongchong Formation in the study area, suggesting an overall sea-level fall from bottom to top. In the lower part of the Posongchong Formation (beds C2-C15), the B/Ga ratio ranges from 3 to 6, indicating a brackish environment. In the middle part of the Posongchong Formation (beds C15 and C16), the B/Ga ratio exceeds 6, indicating that the water body was brackish, with salinity close to that of seawater, which suggests a sea-level rise or transgression occurred during this interval. In the upper part of the Posongchong Formation (beds C17-C20), the B/Ga ratio again falls to between 3 and 6, indicating a return to brackish conditions. However, the B* values for beds C17-C20 are below 200 μg/g, and based on in situ fossil stem evidence, the environment of deposition is interpreted as being freshwater but with some influence of seawater. For beds C21-C28 in the upper part of the Posongchong Formation, the B/Ga ratio remains between 3 and 6, indicating a moderately saline brackish water body, similar to that recorded in beds C2-C15. Based on these findings, it can be concluded that the overall environment of deposition for the Posongchong Formation was brackish, with the middle and lower parts affected by sea level rise that resulted in salinities close to, or even indistinguishable from, those of seawater. Subsequently, as sea level fell, the environment became brackish once more.

4.2. TOC signatures and kerogen macerals

Results of the kerogen maceral and TOC analyses are shown in Fig. S1 and Supplementary Table 1. The TOC content varies from 0.04 % to 3.21 % ($\bar{x}$ = 0.73 %) by weight. The sapropelinite content varies from 6.6 % to 82.7 % ($\bar{x}$ = 34.9 %). The vitrinite content varies from 4 % to 38.1 % ($\bar{x}$ = 21.8 %) and comprises telinite and collinite. The exinite content varies from 10.4 % to 38.4 % ($\bar{x}$ = 23.4 %), the main components of which are sporopollenite, cutinite and suberinite. Inertinite content varies from 1.7 % to 46.9 % ($\bar{x}$= 20.0 %) and is entirely fragmental fusinite.

Kerogen types provide qualitative information about organic matter sources (Meyers and Ishiwatari, 1993a, 1993b). In this study, we use the TI values to evaluate kerogen types. The TI values in beds C17-C19 and C23-C26 are less than 0, indicating type III kerogen, and organic matter is derived principally from terrestrial higher plants. In beds C15 and C16, the TI values are all between 80.3 and 83.8, indicating type I kerogen, with the organic matter composed mainly of algae and aquatic

phytoplankton that was primarily produced in situ in lake and marine settings. In beds C2-C13, the TI values are all between 0 and 40, indicating type II_1 and II_2 kerogen, which generally indicates that organic matter was derived from a mixture of higher plant debris and lower aquatic organisms (Moldowan et al., 1985; Mao et al., 2010). Based on these analyses, we infer that the organic matter in the succession was mainly derived from terrestrial higher plants, followed by mixed sources including algae and lower aquatic organisms.

4.3. Facies analysis

The sedimentary facies recorded in the Posongchong Formation are hereby classified into three facies associations (FAs), each representing a distinct, genetically related set of depositional environments. These settings range from coastal plain/fluviolacustrine (FA A), tidal flat (FA B), and shallow marine (FA C).

4.3.1. Facies Association A: Coastal plain/Fluviolacustrine

Description: Facies Association A comprises three facies (Supplementary Table 2). FA A1 is primarily characterized by interlaminated and thinly interbedded argillaceous and fine-grained sandstones, which exhibit a fining-upward sequence, preserving a diverse array of horizontal lamination and wave ripple cross bedding, with sets generally less than 2 m thick. Sharp basal contacts are usually filled with mudstone clasts, and covered with small amounts of plant debris, with sparse to non-existent bioturbation intensity (BI = 0–1) (Fig. 3). FA A2 comprises mainly interbedded mudstone and siltstone, with sandstone units that are coarsening-upward or sharply bounded, and small-scale cross bedding, ripple cross lamination, and interlamination structures. The interlayer intervals are typically less than 2 m thick and contain plant debris, with well-preserved stems, abundant rooting structures, in situ plant stems, and marine fossils (*Lingula*. sp.) (Fig. 3a, b, c). FA A3 consists primarily of fissile laminated, organic-rich shale, claystone, and siltstone, often containing siderite nodules (Fig. 3e). The interlayer intervals are typically less than 1 m thick and exhibit horizontal lamination (Fig. 3f) and are rich in plant fossil stems and in situ sporangia, as well as marine fossils such as placoderm fish and *Lingula*. sp. brachiopods. The bioturbation intensity and diversity are moderate (BI = 0–4) (Fig. 3d, e, f).

Interpretation: The characteristics of sedimentary structures and the accompanying paleosalinity proxies suggest that FA A represents a tidal-influenced coastal plain environment, predominantly characterized by freshwater conditions (Fig. 3f) but with marine influence evidence by placoderms and lingulid brachiopods. FA A1 is interpreted to record a primarily fluvial channel, possibly affected by tidal processes. This interpretation is supported by the sedimentary structures, the presence of basement erosion surfaces, overlying coarse sediments, and fining-upward facies sequences (Fig. 3f). The underlying argillaceous clastic sandstone was likely deposited by strong currents during periods of high fluvial discharge (Dalrymple et al., 2015; Gugliotta et al., 2016; van Cappelle et al., 2018). The overlying thinly bedded sandstone, which contains fragmented axes and isolated sporangia, records fluvial and high-energy deposits (Fig. 3b). The rich rhythmic stratification (rhythmic bedding) and the presence of brachiopods (*Lingula* sp.) in the sandstone strongly suggest a tidal influence (Figure $3a_1$). The low intensity of bioturbation may be a function of fluctuations in salinity (MacEachern et al., 2005; Buatois et al., 2012), a hypothesis supported by geochemical evidence. The preferential occurrence of biological traces in FA A likely records saltwater intrusion during periods of low river discharge (Gugliotta et al., 2016; Jablonski and Dalrymple, 2016; Collins et al., 2020).

FA A2 and FA A3 are interpreted as floodplain deposits, ranging from

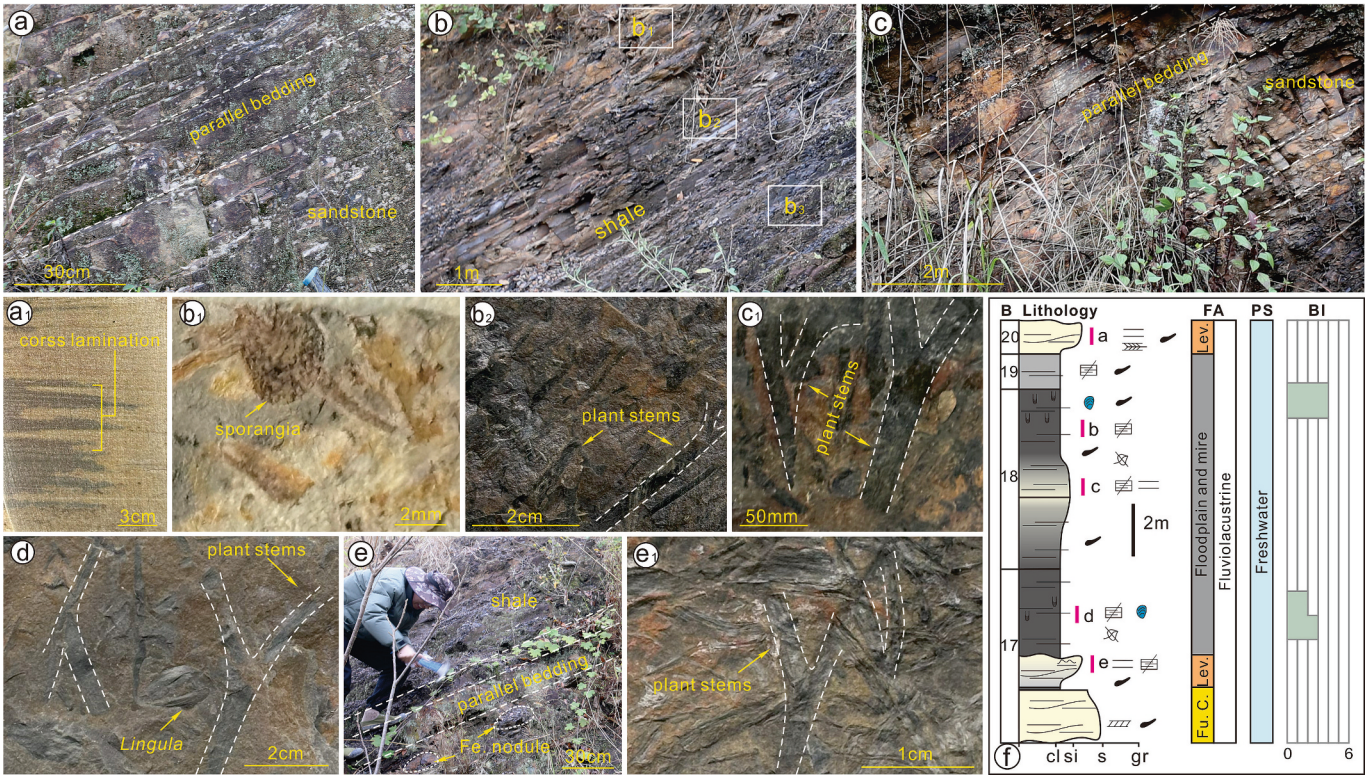

Fig. 3. Examples of Facies Association A (see Supplementary Table 2): a) Parallel bedding in sandstone; a_1) Cross lamination; b) Carbonaceous shale; b_1) Plant sporangia; b_2) Plant stem in mudstone from bed C18; c) Parallel bedding in sandstone; c_1) Plant stem in sandstone from bed C18; d) Plant stem and *Lingula* in sandstone from bed C17; e) Parallel bedding in sandstone and Fe nodule in shale from bed C17; e_1) Plant stem in siltstone from bed C17; f) Stratigraphy of the Zhichang section beds C17-C20 including lithology and facies associations, sedimentary structures, fossils, accessory symbols and paleosalinity. Abbreviations: B = Bed; FA = Facies Association; PS = Paleosalinity; BI = Bioturbation intensity; Lev. = Levee; Fu. C. = Fluvial Channel.

environments proximal to channel margins to more distal locations not influenced by active channel processes. In these areas, sediments were initially deposited by a gradually weakening high-energy sheet flow of water. FA A2 occurs successively in a coarsening-upward depositional sequence, suggesting episodic progradation into an adjacent flooded depression. These conditions result in sandstone bodies with distinct boundary characteristics, which, with the decrease in flow energy, transition to low-energy flow and suspension deposits. Therefore, FA A2 is interpreted as recording levee deposits (Fielding et al., 1993; Michaelsen and Henderson, 2000; Ray and Chakraborty, 2002). FA A3, characterized by coarsening-upward sequences and fine-grained, laterally extensive parallel bedded sandstones, closely resembles crevasse splay deposits (Farrell, 1987; Tye and Coleman, 1989; Jorgensen and Fielding, 1996; Fig. 3c). During flood events, sediments would have been rapidly buried, with plants growing near channel margins in localized areas (Hao and Xue, 2013; Xue et al., 2018; Fig. 3e). In summary, the FA A facies association represents fluvial-dominated fluvio-lacustrine deposits with tidal influences.

4.3.2. *Facies Association B: Tidal flat*

Facies Association B comprises three facies: subtidal (FA B1), intertidal (FA B2) and supratidal (FA B3) deposits (Supplementary Table 2).

Facies Association B1: Supratidal

Description: FA B1 primarily consists of mudstone, claystone and siltstone with a high organic matter content, and geochemical evidence suggests this facies was deposited in a freshwater or brackish environment (Fig. 4f, 5f). The mudstones and siltstones contain a significant number of in-situ plant stem fossils, such as *Zosterophyllum* and *Distichophylum* sp. (Hao and Xue, 2013; Xue et al., 2018; Fig. 4b, e). Layered or blocky yellow to purplish-red siltstone and claystones, which exhibit root traces at the top, contain small amounts of plant debris. These layers also feature visible downward plant roots and rhizomes, with horizontal lamination and small wave-ripple bedding, and the bioturbation intensity is generally low (BI = 0–1) (Fig. 4d, f).

Interpretation: The characteristics of FA B1 suggest that the accumulation of laminated mudstones with root traces is typically associated with low-energy suspension sedimentation in a supratidal zone (Tanavsuu-Milkeviciene and Plink-Bjorklund, 2009; Dalrymple, 2010). The supratidal zone is located higher in the tidal flat setting and this environment is only inundated by a combination of high astronomical and meteorological tides, such as river floods or storm surges (Finkl and Makowski, 2019). The laminated mudstones with plant root traces and bioturbation are typical of supratidal deposits (Dalrymple, 2010; Desjardins et al., 2012; Longhitano et al., 2012). The presence of wave-ripple and flaser bedding likely reflects variations in tidal energy within the supratidal zone (Fig. 4d).

Facies Association B2: Intertidal

Description:FA B2 primarily consists of mudstone, shaly coal, siltstone, and fine sandstone, with a small amount of plant debris (Figs. 4, 5, 7). The sedimentary structures include lenticular bedding, flaser bedding, wave-ripple bedding, and herringbone cross-lamination, which are often disrupted by bioturbation and overlain by mudstone. Thin rhythmic interlayers of mudstone and fine-grained sandstone are only partially preserved, with bioturbation intensity and diversity generally moderate (BI = 0–2) (Figs. 4a, d, f; Fig. 5f). The shaly coal exhibits lamellar and lenticular bedding, with abundant vitrinite, bituminite, and numerous pyrite framboids visible under the microscope (Fig. 5b). The sandstone contains a small amount of plant fossil debris and is poorly sorted, with glauconite minerals present (Figs. 4c, 5e). The layered or blocky mudstone and siltstone have a high organic matter content but few in-situ plant fossils (Fig. 5a).

Interpretation: The characteristics of FA B2 suggest accumulation of tidal bedding and laminated mudstone and sandstones within the intertidal zone (Tanavsuu-Milkeviciene and Plink-Bjorklund, 2009; Dalrymple, 2010; Desjardins et al., 2012; Eide et al., 2016). Intertidal flats are low-relief sandy or muddy areas that are alternately exposed and inundated by astronomical tides (Finkl and Makowski, 2019). The tidal bedding in FA B2 is primarily represented by flaser bedding, lenticular bedding, and wave-ripple bedding in sand/mudstone sequences, indicating deposition in a mixed flat environment (Dalrymple, 2010; Longhitano et al., 2012; Fig. 4a). The presence of rhythmic layering suggests deposition during successive high tides, possibly associated with a meteorological event (Fig. 4a, 7b). The moderate bioturbation intensity indicates the influence of high-energy zones in the intertidal zone (Shen et al., 2023). Tidal inundation and exposure are further evidenced by herringbone cross lamination and the presence of small amounts of plant debris, with red argillaceous interlayers (possibly evaporitic) in the siltstone/sandstone sequences, suggesting deposition

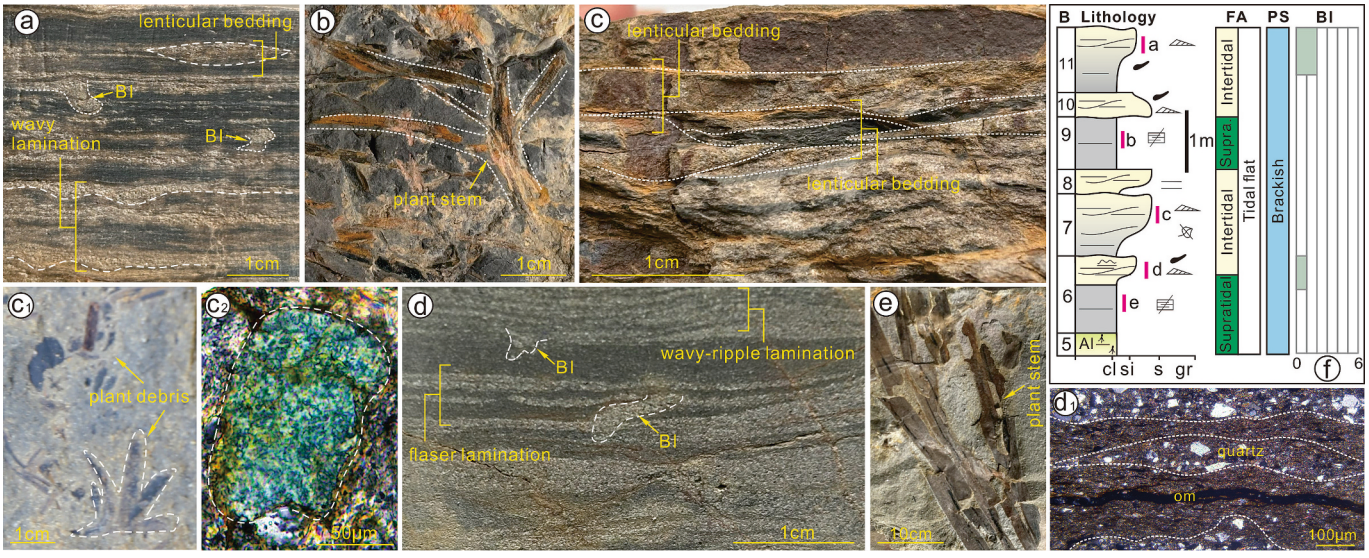

Fig. 4. Examples of Facies Association B (see Supplementary Table 2): a) Lenticular bedding, wave lamination, and bioturbation; b) Plant stem in mudstone from bed C9; c) Lenticular bedding; c_1) Plant debris in siltstone from bed C7; c_2) Glauconite, microstructure characteristics of sandstone in bed C7; d) Flaster lamination and wave-ripple lamination; d_1) Microstructure characteristics of sandstone in bed C6; e) Plant stem in mudstone from bed C6; f) Stratigraphy of the Zhichang section beds C5-C11 including lithology and facies associations, sedimentary structures, fossils, accessory symbols and paleosalinity. Abbreviations: om = Organic matter; B = Bed; FA = Facies Association; PS = Paleosalinity; BI = Bioturbation intensity; Supra. = Supratidal.

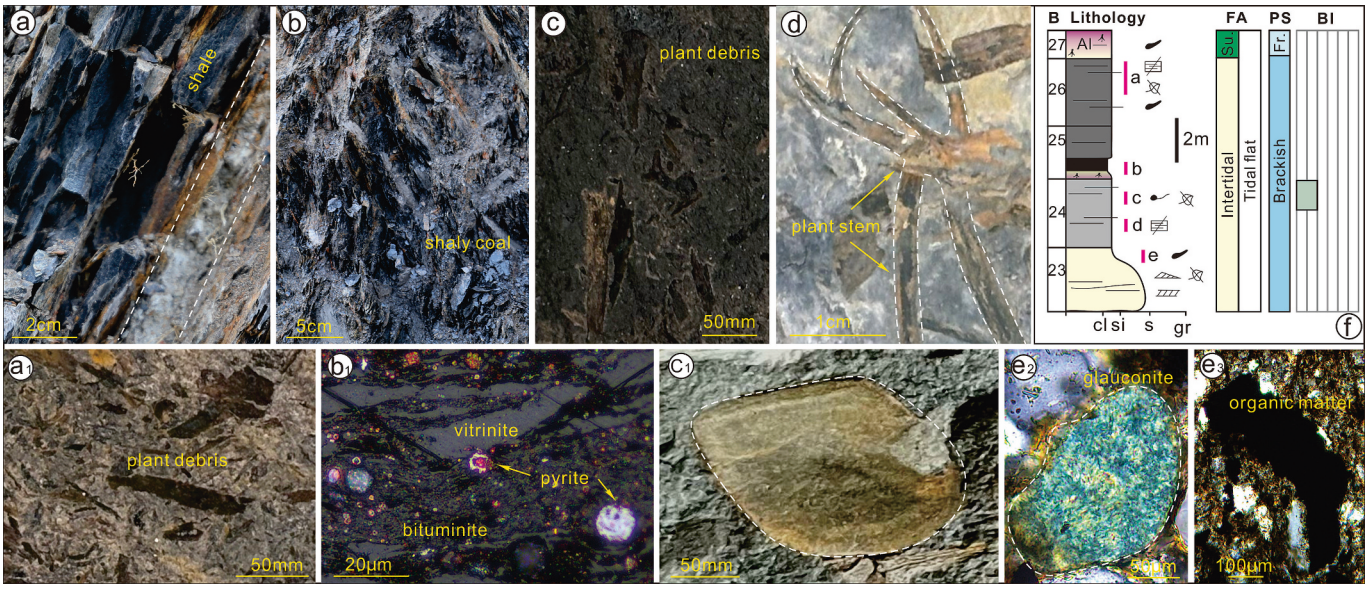

Fig. 5. Examples of Facies Association B (see Supplementary Table 2): a) Shale sequence and tonstein; a_1) Plant debris in mudstone; b) Shaly coal in bed C25; b_1) Organic matter microstructure characteristics; c) Plant debris in mudstone from bed C24; c_1) fossil fragment; d) Plant stem in mudstone from bed C24; e) Plant stem in sandstone from bed C23; e_1) Glauconite microstructure characteristics of sandstone in bed C23; e_2) Organic matter microstructure characteristics of sandstone in bed C23; f) Stratigraphy of the Zhichang section beds C23-C27 including lithology and facies associations, sedimentary structures, fossils, accessory symbols and paleosalinity. Abbreviations: B = Bed; FA = Facies Association; PS = Paleosalinity; BI = Bioturbation intensity; Su. = Supratidal; Fr. = Freshwater.

in a mudflat (Fig. 7b). The upper part of the mudflat may have been occupied by plants, and the interaction of seawater and freshwater could have formed salt marshes (Dalrymple, 2010). The lower part of the mudflat may have formed a depression, which was periodically flooded by saltwater and eventually formed a lagoon.

Facies Association B3: Subtidal

Description:FA B3 primarily consists of gray-black mudstone, siltstone and fine-grained sandstone with little to no organic matter. The sedimentary structures are characterized by parallel laminations, and the paleosalinity index indicates that the water body was of medium salinity (Figs. 6, 7). The deposits are composed of centimeter- to decimeter-scale, very fine to fine-grained sandstone beds that exhibit parallel lamination, wave bedding, and lenticular bedding, embedded within thicker mudstone intervals (Figs. 6, 7). Muddy clasts and plant stems are occasionally found within some layers. Fossil content includes brachiopods (*Lingula* sp.), placoderm fish fragments, and crinoid remains in some layers (Figs. 6a, c; Fig. 7e).

Interpretation: The characteristics of FA B3 suggest that accumulation of lenticular bedding and parallel laminated fine-grained deposition occurred in the subtidal zone (Dalrymple, 2010; Desjardins et al., 2012). The subtidal zone remains continuously submerged and is generally unaffected by astronomical tides (Morales, 2022). The presence of *Lingula* brachiopods, placoderm fish fragments, and crinoid remains indicate a saline, seawater environment prevailed at the time of deposition (Figs. 6a, c; Fig. 7e). The wave and lenticular bedding of sandstone, along with fossil fragments, suggests high-energy conditions, likely influenced by tidal currents and waves (Buatois et al., 2012; Rodríguez et al., 2018). Additionally, the sedimentary features may also

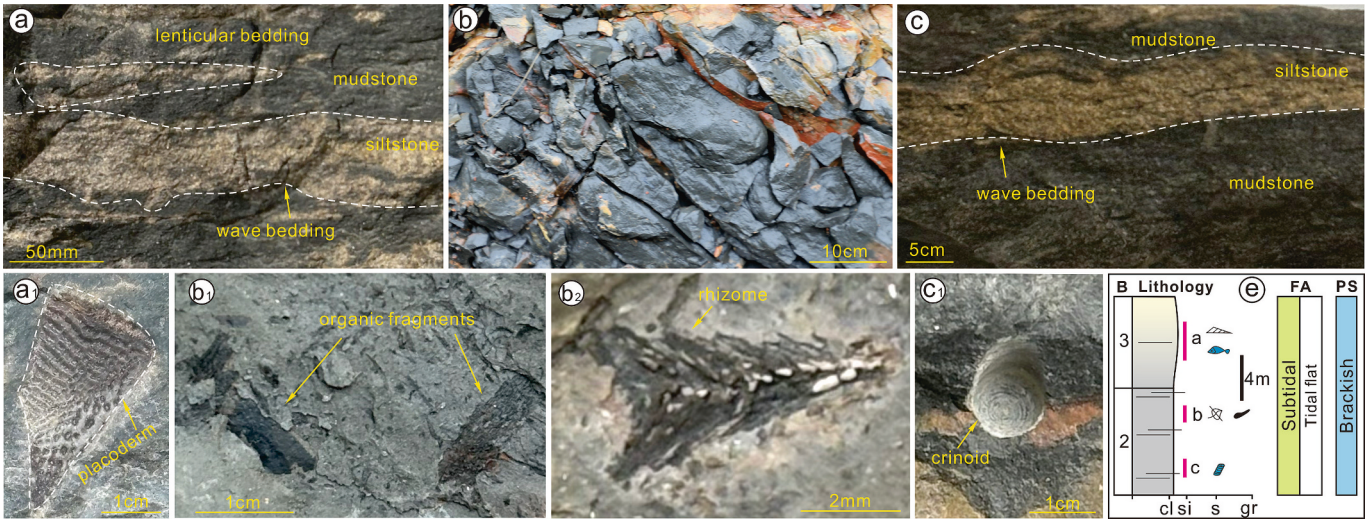

Fig. 6. Examples of Facies Association B (see Supplementary Table 2): a–c) Shale, siltstone and mudstone hand sample; a_1) Placoderm fish skeletal fragments (*Placodermi*); b_1) Plant stem in shale from bed C2; b_2) Rhizome fragment in shale from bed C2; c_1) Crinoid trace fossil; e) Stratigraphy of the Zhichang section beds C2-C3 including lithology and facies associations, sedimentary structures, fossils, accessory symbols and paleosalinity. Abbreviations: B = Bed; FA = Facies Association; PS = Paleosalinity; BI = Bioturbation intensity.

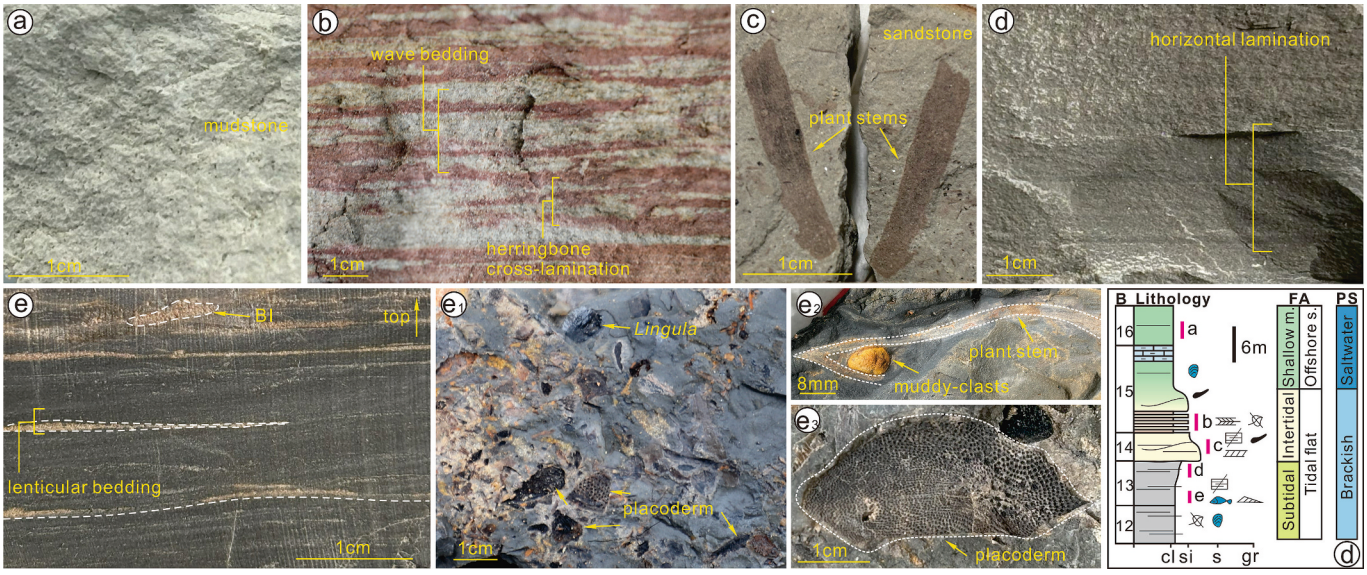

Fig. 7. Examples of Facies Associations B and C (see Supplementary Table 2): a) Mudstone hand sample; b) Herringbone cross lamination; c) Plant debris in shale from bed C14; d) Horizontal lamination in mudstone from bed C15; e) Lenticular bedding in mudstone from bed C13; e_1) Placoderm fish skeletal fragments (*Placodermi*) and *Lingula* fossils; e_2) Plant stem and muddy clasts; e_3) Placoderm fragments; f) Stratigraphy of the Zhichang section beds C12-C16 including lithology and facies associations, sedimentary structures, fossils, accessory symbols and paleosalinity. Abbreviations: B = Bed; FA = Facies Association; PS = Paleosalinity; BI = Bioturbation intensity; m. = Marine; s. = Shelf.

reflect storm-driven deposition (Fürsich and Oschmann, 1993). Taken together, these lines of evidence point to a subtidal, high-energy environment influenced by tidal currents and wave activity.

4.3.3. *Facies Association C: Shallow marine / offshore shelf*

Description: FA C primarily consists of gray-green thick siltstone, argillaceous siltstone, and fine sandstone, with a distinct light gray massive argillaceous limestone layer approximately one meter thick in the middle (Fig. 7a). The siltstone is characterized by wavy cross bedding, lenticular bedding, and other sedimentary structures, but lacks plant fragments. It contains small amounts of organic matter, with abundant bioturbation seen on bedding surfaces. Notable fossil evidence includes the presence of brachiopods (*Lingula* sp.), and geochemical data indicate a saline environment (Fig. 7d).

Interpretation: FA C shows no evidence of proximal sources of coarse-grained sediments, nor signs of wave-disturbed sedimentary structures, and is therefore interpreted as primarily recording shelf conditions below the fair-weather wave base (Morales, 2022). The characteristics of FA C suggest sediment accumulation in a shallow marine environment, with the presence of marine fossils, argillaceous limestone, and evidence of normal salinity (Fielding et al., 2022). The animal fossil fragments and bidirectional cross bedding indicate a high-energy offshore environment, influenced by waves or tides (Buatois et al., 2012; Rodríguez et al., 2018). These features are interpreted to record offshore shelf environments situated between the storm-wave base and fair-weather wave base (MacEachern and Bann, 2008; Fielding et al., 2022).

4.4. *Sea level change*

High-resolution lithofacies analysis reveals that the facies associations FA A to FA C primarily represent coastal plain/fluviolacustrine, tidal flat, and shallow marine environments. These sediments accumulated between the fair-weather wave base and the maximum high-water surface during normal weather conditions. Due to the limited availability of biostratigraphic data, the sea level curves in this study are based on lithological (microfacies) evidence rather than time-based stratigraphy. These findings were then used to reconstruct a comprehensive long-term curve of relative sea-level change in the studied section during the Early Devonian (Fig. 8).

The paleo-environment and paleo-water depth curves, based on facies analysis, reveal two distinct transgressive and regressive cycles during late Pragian-early Emsian (Fig. 8h). The first transgression occurred in the early Pragian, when seawater from the western part of the basin rapidly intruded into the eastern Yunnan region, forming a bay in the study area (Wu et al., 1997). In beds C2 and C3 at the base of the Posongchong Formation, subtidal (FA C) sediments, along with fish fossils, support the interpretation of a transgressive event in the South China Sea. The first regression is recorded by beds C4 and C5, with the depositional environment gradually shifting from subtidal (FA B3) to intertidal (FA B2). A second transgression occurred in the late part of the late Pragian, and is recorded in beds C14–C16 in the middle of the Posongchong Formation. Facies evidence supports a rapid and brief transgression, with the previous intertidal and subtidal environments replaced by a shallow marine environment. This led to a sharp rise in the relative sea level, reaching the maximum depths seen in the study section at that level. A second regression is recorded by bed C17 in the middle part of the Posongchong Formation and this continued into the late Pragian. Comparing the vertical evolution of the depositional environment and long-term sea-level fluctuations of the Posongchong Formation in the Wenshan area with the sea-level curves proposed by Wu et al. (1997) and Ma et al. (2009) reveals that the paleo-water depth in the study area closely mirrors relative sea-level changes in the wider region. This further supports the consistency of the study area's sea-level changes with the global sea-level characteristics during the same period.

5. Discussion

5.1. *Shaly coal accumulation and controlling factors*

Peat mires are typically found in fluvio-lacustrine, deltaic, and coastal plain environments, where complex interactions between tidal and fluvial processes occur (Lv and Chen, 2014; Lv et al., 2022, 2025; Shao et al., 2022; Shen et al., 2024; Zhang et al., 2024). The preservation and degradation of organic matter in peats is influenced by the energy levels of these interactions, including tidal, river, and wave actions, which control the migration, erosion of organic matter, and the supply of terrigenous sediments (Omodeo-Sale et al., 2017). Facies analysis

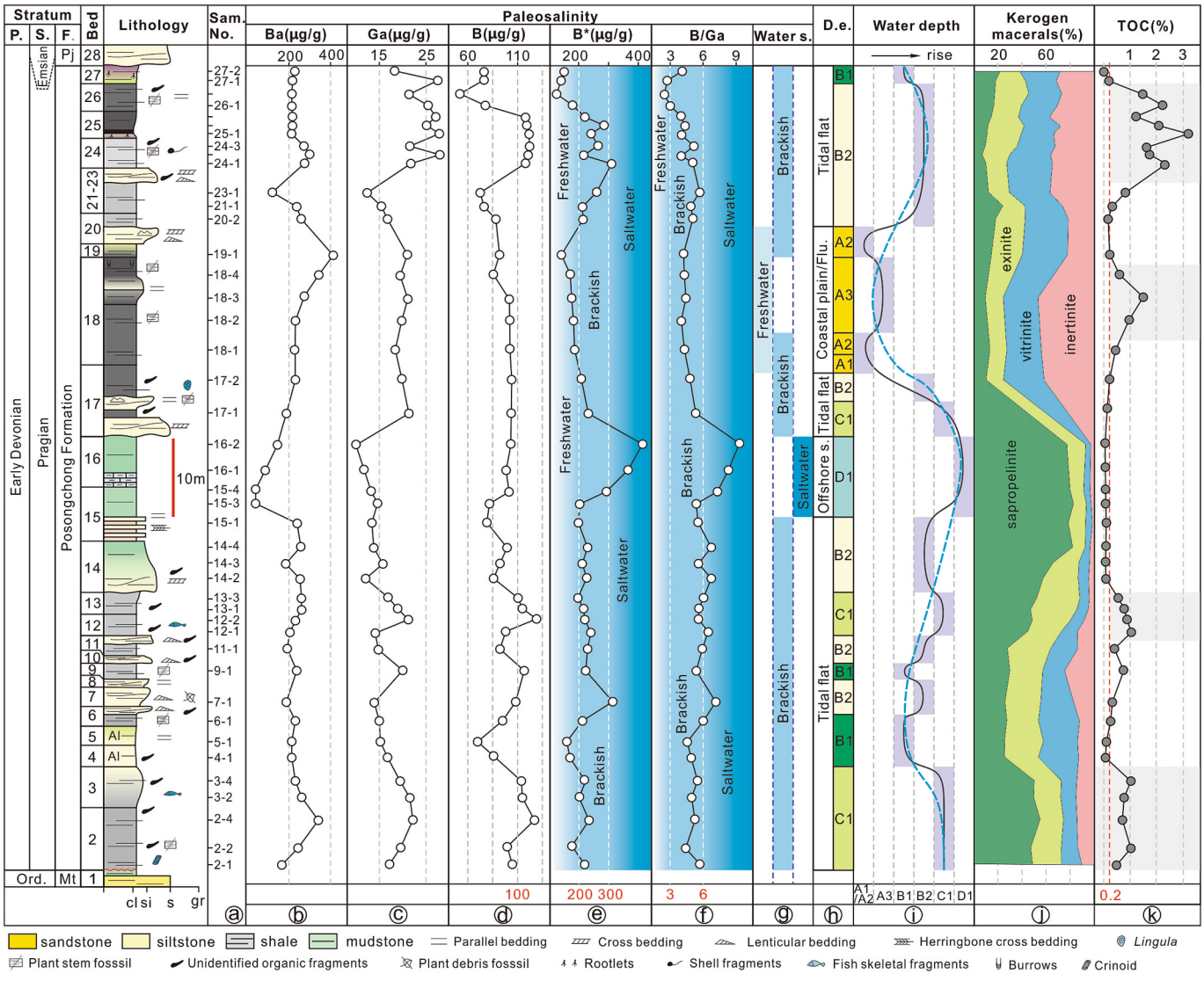

Fig. 8. Depositional environments recorded in the lower part of the Lower Devonian succession in the Zhichang section, showing vertical stacking patterns, correlation of formation boundaries, and available absolute age data. Figure includes facies associations, palaeosalinity, water depth, TOC signatures, kerogen macerals and B/Ga salinity proxy information for the Posongchong Formation (Wei and Algeo, 2020). Abbreviations: P = Period; S. = Stage; Ord. = Ordovician; F. = Formation; Mt. = Meitan; Sam. No. = Sample number; Water s. =Water salinity; D. e. = Depositional environment; Flv. = Fluviolacustrine; s. = Shelf.

indicates that the coal seam at the top of the Posongchong Formation in the study area formed in a supratidal mire environment, which was significantly influenced by tidal and river dynamics. This environment led to the formation of lenticular shaly coal with a glassy luster, approximately 10 cm thick (Fig. 5b). Under microscopic examination, the shaly coal consists primarily of gelocollinite and clastic organic macerals (vitrodetrinite and liptodetrinite), with no inertinite present. The coal also contains high concentrations of pyrite framboids and clay minerals (Figure 5b$_1$). These organic materials are often interspersed with argillaceous materials and organic debris, with alternating layers of gelocollinite and clay. This suggests rapid flocculation and deposition of organic matter under acidic conditions (Fig. 5b).

Previous studies have suggested that primary productivity and the subsequent regulation of organic matter are the most important factors controlling the accumulation and preservation of peat (Diessel, 1992; Banerjee et al., 1996; Bohacs and Suter, 1997; Wadsworth et al., 2002; Shao et al., 2022). Many plant fossils and paleontological remains, including ferns, placoderm fish and *Lingula* sp. brachiopod marine fossils and other plankton, have been identified in the late Pragian strata, indicating the importance of accumulation in peat under specific conditions. Crustal subsidence and sea-level fluctuations are key factors controlling changes in accommodation space, influencing peat accumulation (Shao et al., 2022; Shen et al., 2023). During the late Pragian-early Emsian, the South China Plate experienced relatively stable tectonic conditions, and sedimentation rates likely remained steady over short periods (Wu et al., 1997). According to global sea-level curves for the Early Devonian, two significant transgressions and regressions occurred during the late Pragian-early Emsian, and the sedimentary sequence of the Posongchong Formation reflects the influence of these sea-level changes. The late Pragian-early Emsian climate was warm and humid, creating an ideal environment for the formation of shaly coal at the top of the Posongchong Formation (Slavík et al., 2016; Slavík and Hladil, 2020). This accumulation occurred during a period of falling sea levels, but was strongly influenced by tidal actions, leading to the development of a broad, flat coastal plain where peat mires began to form. During deposition, temporary subsidence and sea-level changes reached a balance. However, this equilibrium between accommodation space and peat accumulation could not be sustained over extended time intervals, eventually leading to the formation of the shaly coal of the Posongchong Formation (Fig. 9).

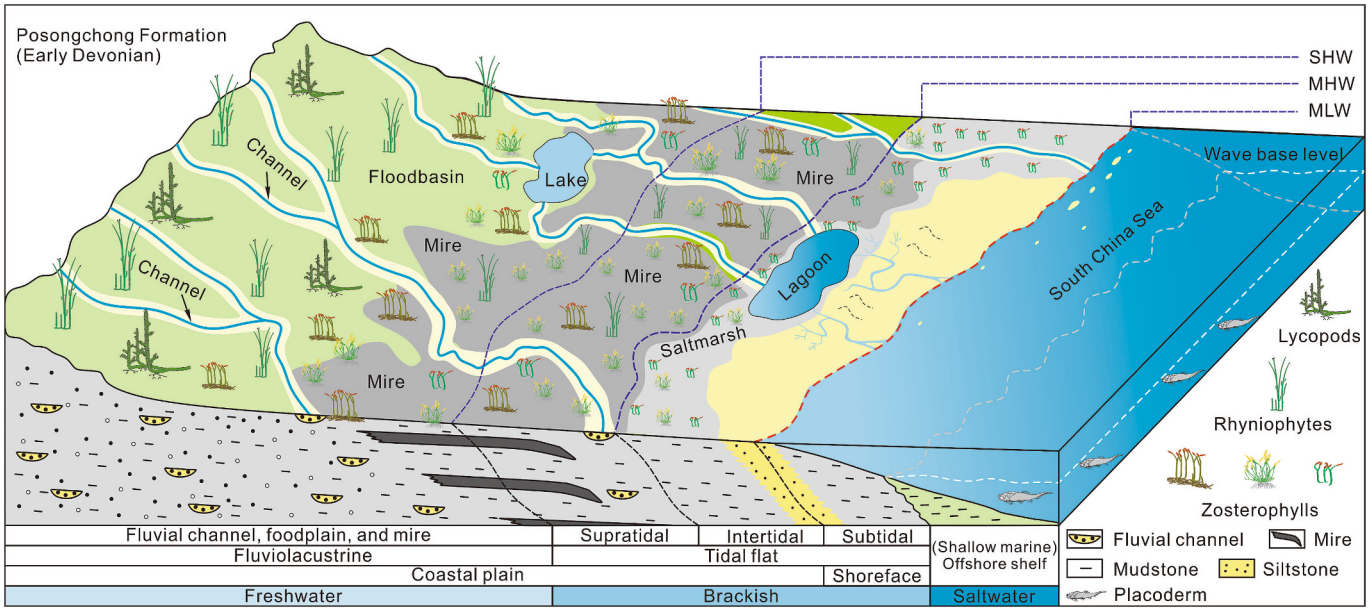

Fig. 9. Schematic diagram showing the organic matter accumulation models for the Posongchong Formation. Abbreviations: EHW = Extreme High Water Level; MHW = Mean High Water Level; MLW = Mean Low Water Level.

5.2. *Drivers of Early Devonian terrestrial organic carbon burial*

Facies analysis reveals that organic carbon accumulation occurs in supratidal, subtidal, intertidal lagoon, and fluviolacustrine environments (Figs. 8, 9). The results indicate that the average organic carbon content is highest in sediments deposited in intertidal lagoon

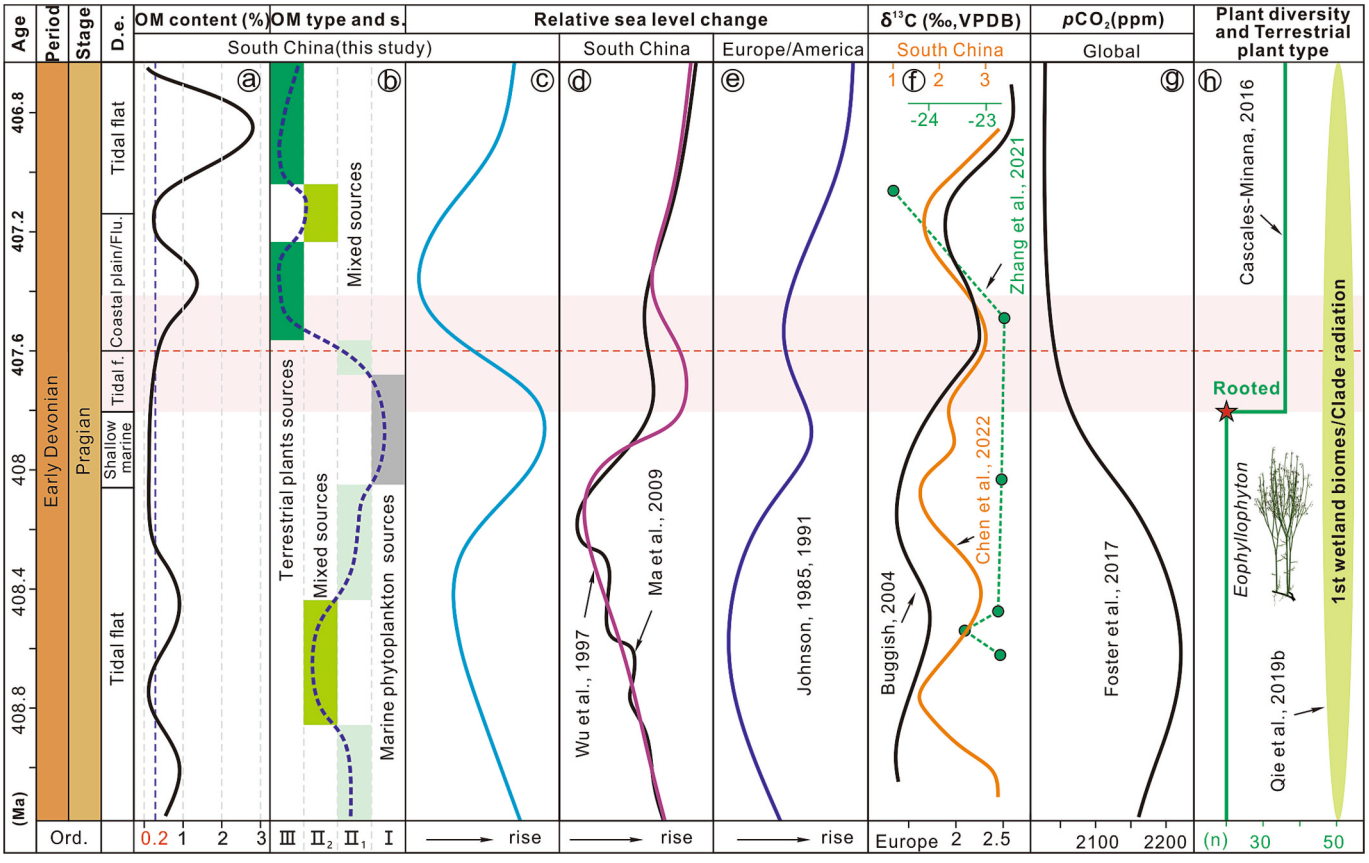

Fig. 10. Correlation of depositional environments, organic matter content, organic matter type, relative sea level change (Johnson et al., 1985, 1991; Wu et al., 1997; Ma et al., 2009), carbon isotope (Buggisch and Mann, 2004; Chen et al., 2024), pCO_2 (Foster et al., 2017), plant diversity and terrestrial plant types (Cascales-Miñana, 2016) for the Early Devonian Posongchong Formation. Abbreviations: D. e = Depositional environment; Ord. = Ordovician; OM = Organic matter; OM type and s. = OM type and source; Tidal f. = Tidal flat; Flv. = Fluviolacustrine.

environments ($\bar{x}$ = 2.5 %), followed by the fluviolacustrine environments ($\bar{x}$ = 1.8 %) and the subtidal zone ($\bar{x}$ = 1.1 %). Among these environments, the intertidal lagoon environment exhibits significantly higher organic carbon content compared to other aquatic environments (Supplementary Table 1; Fig. 8j).

In the study area, the relatively stable coastal environment and the initial stages of plant terrestrialization played a crucial role in organic matter accumulation (Figs. 9, 10). Total Organic Carbon (TOC) provides valuable insights into the sedimentary environment (Tissot and Welte, 1984; Meyers and Ishiwatari, 1993a, 1993b). In the study area, organic matter is mainly derived from terrestrial higher plants, followed by algae and lower aquatic organisms (Fig. 10a, b). Organic matter in marine environments may be more resistant to degradation, leading to higher TOC preservation after subsequent exposure. By correlating sea level changes with organic matter content, the results further suggest that environments of differing salinities exhibit varying organic matter concentrations. Specifically, the organic matter content in sediments that accumulated in freshwater and brackish water environments is significantly higher than those in marine environments (Fig. 8). Notably, closed-water environments appear to be particularly favorable for organic carbon enrichment.

It is believed that the transport of suspended debris from coastal plains to the basin plays a significant role in the rapid accumulation of organic matter (Milliman and Syvitski, 1992). Intertidal lagoons, characterized by relatively still waters, provide a reducing environment where the complex interaction between tidal currents and rivers occurs over extended periods (Slattery et al., 2006). This environment allows for the accumulation of sediments, which are more conducive to the preservation of organic matter in earlier sediments. The upper part of the intertidal zone, a typical saltmarsh environment with higher terrain and low salinity, is less affected by seawater and wet conditions, thereby favoring the preservation of organic matter (Gonneea et al., 2019; Byrd and Kelly, 2006; Kirwan et al., 2013). In the subtidal zone, the relatively high organic matter content can be attributed to the deeper water and higher salinity conditions during the early stages of sedimentation, which facilitated the burial and preservation of both sediments and organic matter brought in by terrigenous inputs.

The highest TOC values and preponderance of type III kerogen from terrestrial plants sources at the top of the Posongchong Formation correspond to intervals of higher water levels, indicating that the change of sea level is conducive to the enrichment of organic matter (Fig. 10a, b, c). This sea level change event has been recorded in many parts of the world. In Europe and America, the rise and the fall of sea level appears to have been synchronous with that in South China (Wu et al., 1997; Ma et al., 2009; Fig. 10d, e). We compiled a low latitude composite $\delta^{13}C$ curve for the Early Devonian period, using the late Pragian-early Emsian database of South China (Zhang et al., 2021; Chen et al., 2024) and Europe (Buggisch and Mann, 2004). This record suggests that the sea level changes, and the onset of terrestrial organic carbon burial were synchronous at that time. However, some scholars question whether the lower organic carbon content in Early Devonian strata reflects terrestrial carbon burial (Edwards et al., 1979; Xue et al., 2022). To address this issue, we examine it from the perspective of historical context and plant terrestrialization (Fig. 10h). The Early Devonian was a time of clade explosion in plants, dominated by vascular plants with relatively undeveloped xylems, making them more prone to degradation and less likely to preserve organic matter (Gensel and Edwards, 2001; Qie et al., 2019b, 2021a, 2021b; Xue et al., 2022, 2023a, 2023b). Plants absorb CO_2 from the atmosphere through photosynthesis and convert inorganic carbon into organic compounds for storage in the plant body. This trend is supported by changes in the organic carbon isotopes of plants (Zhang et al., 2021), global inorganic carbon isotope records and pCO_2 data (Buggisch and Mann, 2004; Foster et al., 2017; Lenton et al., 2018; Chen et al., 2024; Fig. 10g, h). The emergence and diversification of land plants significantly increased the production of organic carbon and thus the terrestrialization of the land surface by plants undoubtedly promoted the formation and expansion of the terrestrial carbon pool (Cascales-Miñana, 2016; Qie et al., 2019b; Xue et al., 2022; Xue et al., 2023a, 2023b). Based on the above considerations, we argue that the Early Devonian Posongchong Formation serves as a typical example of early terrestrial carbon burial, which holds significant implications for understanding the processes of plant terrestrialization.

6. Conclusions

(1) Paleosalinity indices (B* and B/Ga) indicate that deposition of the Posongchong Formation occurred in a range of freshwater, brackish, and saltwater environments. Based on the characteristics of paleosalinity and sedimentary structures, fluviolacustrine (FA A), tidal flat (FA B), and shallow marine (FA C) facie associations have been identified in the Posongchong Formation. Sea level changes based on these facies associations reveal two episodes of sea level rise. This further supports the consistency of the study area's sea level record with global patterns during the same period.

(2) Total Organic Carbon (TOC) and kerogen maceral analyses indicate an increase in terrestrial organic carbon content sourced from terrestrial higher plants and phytoplankton; The highest TOC values and preponderance of type III kerogen in the Posongchong Formation correspond to intervals of higher water levels, indicating that the change of sea level is conducive to the enrichment of organic matter. At the same time, the formation of shaly coal and carbonaceous shales in a stable coastal environment further indicates the influence of higher terrestrial plants on organic matter accumulation.

CRediT authorship contribution statement

Lusheng Yin: Writing – review & editing, Writing – original draft, Investigation, Formal analysis, Conceptualization. **Minfang Yang:** Writing – review & editing, Writing – original draft, Investigation, Formal analysis, Conceptualization. **Jing Lu:** Writing – review & editing, Writing – original draft, Investigation, Formal analysis, Conceptualization. **Ziyu Ling:** Writing – review & editing, Writing – original draft, Investigation, Formal analysis. **Xiaoyu Hu:** Writing – review & editing, Writing – original draft, Investigation, Formal analysis. **Xiao Bian:** Writing – review & editing, Writing – original draft, Investigation. **Kai Zhou:** Writing – review & editing, Writing – original draft, Investigation. **Peixin Zhang:** Writing – review & editing, Writing – original draft, Investigation, Formal analysis. **Le Liu:** Writing – review & editing, Writing – original draft, Investigation. **Longyi Shao:** Writing – review & editing, Writing – original draft, Investigation, Conceptualization. **Jason Hilton:** Writing – review & editing, Writing – original draft, Investigation, Formal analysis, Conceptualization. **David P.G. Bond:** Writing – review & editing, Writing – original draft, Investigation, Formal analysis.

Declaration of competing interest

The authors declare that they have no known competing financial interests or personal relationships that could have appeared to influence the work reported in this paper.

Acknowledgments

We are grateful to Suping Peng and Shifeng Dai (China University of Mining and Technology Beijing) for their comments on earlier versions of the manuscript. Financial support was provided by the National Key Research and Development Program of China (2022YFF0800200), the National Natural Science Foundation of China (Grant nos. 42172196, 41772161, and 41472131). DPGB and JH acknowledge NERC Standard Grant NE/V001639/1.

Appendix A. Supplementary data

Supplementary data to this article can be found online at https://doi.org/10.1016/j.palaeo.2025.113039.

Data availability

The authors confirm that all data necessary for supporting the scientific findings of this paper have been provided.

References

Algeo, T.J., Scheckler, S.E., 1998. Terrestrial-marine teleconnections in the Devonian: links between the evolution of land plants, weathering processes, and marine anoxic events. Phil. Trans. Roy. Soc. B: Biol. Sci. 353 (1365), 113–130.

Algeo, T.J., Scheckler, S.E., Maynard, J.B., 2001. Effects of the middle to late Devonian spread of vascular land plants on weathering regimes, marine biotas, and global climate. In: Gensel, P.G., Edwards, D. (Eds.), Plants Invade the Land: Evolutionary and Environmental Perspectives. Columbia University Press, New York, pp. 213–236.

Bábek, O., Famera, M., Hladil, J., Kapusta, J., Weinerová, H., Simicek, D., Slavík, L., Durisova, J., 2018a. Origin of red pelagic carbonates as an interplay of global climate and local basin factors: insight from the Lower Devonian of the Prague Basin, Czech Republic. Sediment. Geol. 364, 71–88.

Bábek, O., Famera, M., Simicek, D., Weinerová, H., Hladil, J., Kalvoda, J., 2018b. Sea-level changes vs. organic productivity as controls on Early and Middle Devonian bioevents: Facies and gamma-ray based sequence-stratigraphic correlation of the Prague Basin, Czech Republic. Glob. Planet. Chang. 160, 75–95.

Banerjee, I., Kalkreuth, W., Davies, E.H., 1996. Coal seam splits and transgressive-regressive coal couplets: a key to stratigraphy of high-frequency sequences. Geology 24, 1001–1004.

Bateman, R.M., Crane, P.R., DiMichele, W.A., Kenrick, P., Rowe, N.P., Speck, T., Stein, W.E., 1998. Early evolution of land plants: phylogeny, physiology, and ecology of the primary terrestrial radiation. Annu. Rev. Ecol. Syst. 29, 263–292.

Bohacs, K.M., Suter, J.R., 1997. Sequence stratigraphic distribution of coaly rocks: fundamental controls and paralic examples. AAPG Bull. 81, 1612–1639.

Breiter, K., Gardenová, N., Kanický, V., Vaculovič, T., 2013. Gallium and germanium geochemistry during magmatic fractionation and post-magmatic alteration in different types of granitoids: a case study from the Bohemian Massif (Czech Republic). Geology 64 (3), 171–180.

Buatois, L.A., Santiago, N., Herrera, M., Plink-Bjorklund, P.E., Steel, R.J., Espin, M., Parra, K., 2012. Sedimentological and ichnological signatures of changes in wave, river and tidal influence along a Neogene tropical deltaic shoreline. Sedimentology 59, 1568–1612.

Buggisch, W., Joachimski, M.M., 2006. Carbon isotope stratigraphy of the Devonian of Central and Southern Europe. Palaeogeogr. Palaeoclimatol. Palaeoecol. 240 (1–2), 68–88.

Buggisch, W., Mann, U., 2004. Carbon isotope stratigraphy of Lochkovian to Eifelian limestones from the Devonian of central and southern Europe. Int. J. Earth Sci. 93 (4), 521–541.

Buggisch, W., Joachimski, M.M., Sevastopulo, G., Morrow, J.R., 2008. Mississippian δ^{13}Ccarb and conodont apatite δ^{18}O records—their relation to the late Palaeozoic Glaciation. Palaeogeogr. Palaeoclimatol. Palaeoecol. 268 (3–4), 273–292.

Burrett, C., Zaw, K., Meffre, S., Lai, C.K., Khositanont, S., Chaodumrong, P., Udchachon, M., Ekins, S., Halpin, J., 2014. The configuration of Greater Gondwana—evidence from LA ICPMS, U-Pb geochronology of detrital zircons from the Palaeozoic and Mesozoic of Southeast Asia and China. Gondwana Res. 26, 31–51.

Byrd, K.B., Kelly, M., 2006. Salt marsh vegetation response to edaphic and topographic changes from upland sedimentation in a Pacific estuary. Wetlands 26 (3), 813–829.

Carroll, A.R., Bohacs, K.M., 1999. Stratigraphic classification of ancient lakes: balancing tectonic and climatic controls. Geology 27, 99–100.

Cascales-Miñana, B., 2016. Apparent changes in the Ordovician−Mississippian plant diversity. Rev. Palaeobot. Palynol. 227, 19–27.

Cascales-Miñana, B., Xue, J.Z., Rial, G., Gerrienne, P., Huang, P., Steemans, P., 2017. Revisiting the spore assemblages from the Lower Devonian Posongchong Formation of Wenshan, Yunnan Province, southwestern China. Earth Environ. Sci. Trans. R. Soc. Edinburgh 108 (4), 339–354.

Chen, Z.Y., Chen, Z.L., Zhang, W.G., 1997. Quaternary stratigraphy and trace-element indices of the Yangtze Delta, Eastern China, with special reference to marine transgressions. Quat. Res. 47 (2), 181–191.

Chen, B., Ma, X.P., Mills, B.J.W., Qie, W., Joachimski, M.M., Shen, S., Wang, C., Xu, H., Wang, X., 2021. Devonian paleoclimate and its drivers: a reassessment based on a new conodont δ^{18}O record from South China. Earth-Sci. Rev. 222, 103814.

Chen, B., Zhang, M.Q., Qie, W.K., Liang, K., Lu, J.F., Joachimski, M.M., Ma, X.P., 2024. Carbon and conodont apatite oxygen isotope records from the Alengchu section in western Yunnan and their paleoclimatic and paleogeographic implications. Palaeoworld 33, 559–569.

Collins, D.S., Johnson, H.D., Baldwin, C.T., 2020. Architecture and preservation in the fluvial to marine transition zone of a mixed-process humid-tropical delta: Middle Miocene Lambir Formation, Baram Delta Province, north-West Borneo. Sedimentology 67, 1–46.

Dalrymple, R.W., 2010. Tidal depositional systems. In: James, N.P., Dalrymple, R.W. (Eds.), Facies Models, vol. 4. Geological Association of Canada, pp. 201–231.

Dalrymple, R.W., Kurcinka, C.E., Jablonski, B.V.J., Ichaso, A.A., Mackay, D.A., 2015. Deciphering the relative importance of fluvial and tidal processes in the fluvialmarine transition. In: Ashworth, P.J., Best, J.L., Parsons, D.R. (Eds.), Fluvial-Tidal Sedimentology, Development in Sedimentology, vol. 68, pp. 3–45.

Davies, N.S., Gibling, M.R., 2010. Cambrian to Devonian evolution of alluvial systems: the sedimentological impact of the earliest land plants. Earth-Sci. Rev. 98 (3/4), 171–200.

Desjardins, P.R., Buatois, L.A., Mangano, M.G., 2012. Tidal flats and subtidal sand bodies. In: Knaust, D., Bromley, R.G. (Eds.), Trace Fossils as Indicators of Sedimentary Environments, Developments in Sedimentology, vol. 64, pp. 529–561.

Diessel, C.F.K., 1992. Coal-Bearing Depositional Systems. Springer Verlag, Berlin, p. 721.

Edwards, D., Bassett, M.G., Rogerson, E.C.W., 1979. The earliest vascular land plants: continuing the search for proof. Lethia 12, 313–324.

Eide, C.H., Howell, J.A., Buckley, S.J., Martinius, A.W., Oftedal, B.T., Henstra, G.A., Marzo, M., 2016. Facies model for a coarse-grained, tide-influenced delta: Gule Horn Formation (Early Jurassic), Jameson Land, Greenland. Sedimentology 63, 1474–1506.

Fang, Z.J., Cai, C.Y., Wang, Y., Li, X.X., Wang, C.Y., Geng, L.Y., Wang, S.Q., Gao, L.D., Wang, N.Z., Li, D.Y., 1994. New advance in the study of the Silurian–Devonian boundary in Qujing, east Yunnan. J. Stratigr. 18, 81–90.

Farrell, K.M., 1987. Sedimentology and facies architecture of overbank deposits of the Mississippi river, false river region, Louisiana. SEPM Spec. Pub. 39, 111–120.

Fielding, C.R., Frank, T.D., Savatic, K., Mays, C., Mcloughlin, S., Vajda, V., Nicoll, R.S., 1993. Fluvial response to foreland basin overfilling; the Late Permian Rangal coal measures in the Bowen Basin, Queensland, Australia. Sediment. Geol. 85, 475–497.

Fielding, C.R., Frank, T.D., Savatic, K., Mays, C., Mcloughlin, S., Vajda, V., Nicoll, R.S., 2022. Environmental change in the late Permian of Queensland, NE Australia: the warmup to the end–Permian Extinction. Palaeogeogr. Palaeoclimatol. Palaeoecol. 594, 110936.

Finkl, C.W., Makowski, C., 2019. Encyclopedia of Coastal Science, 2. Springer, Berlin, pp. 1805–1808.

Foster, G.L., Royer, D.L., Lunt, D.J., 2017. Future climate forcing potentially without precedent in the last 420 million years. Nat. Commun. 8, 14845.

Frýda, J., Lehnert, O., Joachimski, M.M., Männik, P., Kubajko, M., Mergl, M., Farkas, J., Frýdová, B.J., 2021. The Mid–Ludfordian (late Silurian) Glaciation: a link with global changes in ocean chemistry and ecosystem overturns. Earth-Sci. Rev. 220, 103652.

Fürsich, F.T., Oschmann, W., 1993. Shell beds as tools in basin analysis: the Jurassic of Kachchh, western India. J. Geol. Soc. Lond. 150, 169–185.

Gensel, P.G., Edwards, D., 2001. Plants in time and space: linking palaeobotany and land plant phylogeny. Biol. Rev. 76 (4), 403–437.

Gerienne, P., Servais, T., Vecoli, M., 2016. Plant evolution and terrestrialization during Paleozoic times–the phylogenetic context. Rev. Palaeobot. Palynol. 227, 4–18.

Gibling, M.R., Davies, N.S., 2012. Palaeozoic landscapes shaped by plant evolution. Nat. Geosci. 5, 99–105.

Gonneea, M.E., Maio, C.V., Kroeger, K.D., Hawkes, A.D., Mora, J., Sullivan, R., Madsen, S., Buzard, R.M., Cahill, N., Donnelly, J.P., 2019. Salt marsh ecosystem restructuring enhances elevation resilience and carbon storage during accelerating relative sea-level rise. Estuar. Coast. Shelf Sci. 217, 56–68.

Gugliotta, M., Flint, S.S., Hodgson, D.M., Veiga, G.D., 2016. Recognition criteria, characteristics and implications of the fluvial to marine transition zone in ancient deltaic deposits (Lajas Formation, Argentina). Sedimentology 63, 1971–2001.

Hao, S.G., Xue, J.Z., 2013. The Early Devonian Posongchong Flora of Yunnan-A Contribution to an Understanding of the Evolution and Early Diversification of Vascular Plants. Science Press, Beijing, pp. 1–366.

Harder, H., 1970. Boron content of sediments as a tool in facies analysis. Sediment. Geol. 4, 153–175.

Hawkins, D.B., Roy, R., 1963. Distribution of trace elements between clays and zeolites formed by hydrothermal alteration of synthetic basalts. Geochim. Cosmochim. Acta 27 (7), 785–795.

Husson, J.M., Schoene, B., Bluher, S., Maloof, A.C., 2016. Chemostratigraphic and U-Pb geochronologic constraints on carbon cycling across the Silurian-Devonian boundary. Earth Planet. Sci. Lett. 436, 108–120.

Jablonski, B.V.J., Dalrymple, R.W., 2016. Recognition of strong seasonality and climatic cyclicity in an ancient, fluvially dominated, tidally influenced point bar: Middle McMurray Formation, Lower Steepbank River, northeastern Alberta, Canada. Sedimentology 63, 552–585.

Jin, S.Y., Shen, A.J., Chen, Z.L., Lu, J.M., Wei, M., Wang, Y.Q., Xie, F., 2005. Mixed Biostratigraphy of Devonian in Wenshan, Yunnan. Petroleum Industry Press, Beijing.

Joachimski, M.M., Buggisch, W., 2002. Conodont apatite δ^{18}O signatures indicate climatic cooling as a trigger of the late Devonian mass extinction. Geology 30 (8), 711–714.

Joachimski, M.M., Pancost, R.D., Freeman, K.H., Ostertag-Henning, C., Buggisch, W., 2002. Carbon isotope geochemistry of the Frasnian–Famennian transition. Palaeogeogr. Palaeoclimatol. Palaeoecol. 181 (1–3), 91–109.

Joachimski, M.M., Breisig, S., Buggisch, W., Talent, J.A., Mawson, R., Gereke, M., Morrow, J.R., Day, J., Weddige, K., 2009. Devonian climate and reef evolution: insights from oxygen isotopes in apatite. Earth Planet. Sci. Lett. 284 (3–4), 599–609.

Johnson, J.G., Klapper, G., Sandberg, C.A., 1985. Devonian eustatic fluctuations in Euramerica. Geol. Soc. Am. Bull. 96 (5), 567–587.

Johnson, J.G., Sandberg, C.A., Poole, F.G., 1991. Devonian lithofacies of Western United States. Geology 2, 235–239.

Jorgensen, P.J., Fielding, C.R., 1996. Facies architecture of alluvial floodbasin deposits; three-dimensional data from the Upper Triassic Callide coal measures of east-Central Queensland, Australia. Sedimentology 43, 479–495.
Keren, R., Mezuman, U., 1981. Boron adsorption by clay minerals using a phenomenological equation. Clay Clay Miner. 29 (3), 198–204.
Kirwan, M.L., Langley, J.A., Guntenspergen, G.R., Megonigal, J.P., 2013. The impact of sea-level rise on organic matter decay rates in Chesapeake Bay brackish tidal marshes. Biogeosciences 10, 1869–1876.
Lai, C.K., Meffre, S., Crawford, A.J., Zaw, K., Halpin, J.A., Xue, C.D., Salam, A., 2014. The Central Ailaoshan ophiolite and modern analogs. Gondwana Res. 26, 75–88.
Lenton, T.M., Crouch, M., Johnson, M., Pires, N., Dolan, L., 2012. First plants cooled the Ordovician. Nat. Geosci. 5 (2), 86–89.
Lenton, T.M., Daines, S.J., Mills, B.J.W., 2018. COPSE reloaded: an improved model of biogeochemical cycling over Phanerozoic time. Earth-Sci. Rev. 178, 1–28.
Liao, W.H., Ruan, Y.P., 2003. Devonian biostratigraphy of China. In: Zhang, W.T., Chen, P.J., Palmer, A.R. (Eds.), Biostratigraphy of China. Science Press, Beijing, pp. 237–279.
Longhitano, S.G., Mellere, D., Steel, R.J., Ainsworth, R.B., 2012. Tidal depositional systems in the rock record: a review and new insights. Sediment. Geol. 279, 2–22.
Lu, J.F., Chen, X.Q., 2016. New insights into the base of the Emsian (Lower Devonian) in South China. Geobios 49, 459–467.
Lv, D.W., Chen, J.T., 2014. Depositional environments and sequence stratigraphy of the Late Carboniferous – Early Permian coal-bearing successions (Shandong Province, China): Sequence development in an epicontinental basin. J. Asian Earth Sci. 9, 16–30.
Lv, D., Wang, L., Isbell, J.L., Lu, C., Li, P., Wang, Y., Zhang, Z., 2022. Records of chemical weathering and volcanism linked to paleoclimate transition during the Late Paleozoic Icehouse. Glob. Planet. Chang. 217, 103934.
Lv, D.W., Zhao, Y.T., Steel, R.J., Jia, H.B., Raji, M., Zhang, Z.H., Ju, L., Gong, L.H., Wang, X.Y., 2025. Massive organic carbon burial in the North China Basin is a main contributor to peak Late Paleozoic Ice Age in early Asselian. Earth Planet. Sci. Lett. 661, 119370.
Ma, X.P., Liao, W.H., Wang, D.M., 2009. The Devonian system of China, with a discussion on sea–level change in South China. In: Königshof, P. (Ed.), Devonian Change: Case Studies in Palaeogeography and Palaeoecology, vol. 314. Geological Society of London, pp. 241–262.
MacEachern, J.A., Bann, K.L., 2008. The role of ichnology in refining shallow marine facies models. In: Hampson, G.J., Steel, R.J., Burgess, P.M., Dalrymple, R.W. (Eds.), Recent Advances in Models of Siliciclastic Shallow–Marine Stratigraphy, vol. 90. SEPM Society for Sedimentary Geology, pp. 73–116.
MacEachern, J.A., Bann, K.L., Bhattacharya, J.P., Howell, C.D., 2005. Ichnology of deltas: Organism responses to the dynamic interplay of rivers, waves, storms, and tides. In: Gioson, L., Bhattacharya, J.P. (Eds.), River Deltas: Concepts Models and Examples, vol. 83. SEPM Society for Sedimentary Geology, pp. 49–85.
Małkowski, K., Racki, G., 2009. A global biogeochemical perturbation across the Silurian–Devonian boundary: ocean-continent-biosphere feedbacks. Palaeogeogr. Palaeoclimatol. Palaeoecol. 276 (1), 244–254.
Mao, J., Fang, X., Lan, Y., Schimmelmann, A., Mastalerz, M., Xu, L., Schmidt-Rohr, K., 2010. Chemical and nanometer-scale structure of kerogen and its change during thermal maturation investigated by advanced solid-state ^{13}C NMR spectroscopy. Geochim. Cosmochim. Acta 74, 2110–2127.
McMahon, W.J., Davies, N.S., 2018. Evolution of alluvial mudrock forced by early land plants. Science 359 (6379), 1022–1024.
Meyers, P.A., Ishiwatari, R., 1993a. The early diagenesis of organic matter in lacustrine sediments. In: Engel, M.H., Macko, S.A. (Eds.), Organic Geochemistry. Topics in Geobiology 11. Springer, Boston, MA, pp. 185–209.
Meyers, P.A., Ishiwatari, R., 1993b. Lacustrine organic geochemistry an overview of indicators of organic matter sources and diagenesis in lake sediments. Org. Geochem. 20 (7), 867–900.
Michaelsen, P., Henderson, R.A., 2000. Facies relationships and cyclicity of high–latitude, Late Permian coal measures, Bowen Basin, Australia. Int. J. Coal Geol. 44, 19–48.
Milliman, J.D., Syvitski, J.P.M., 1992. Geomorphic/tectonic control of sediment discharge to the ocean: the importance of small mountainous rivers. Geology 100 (5), 525–544.
Moldowan, J.M., Seifert, W.K., Gallegos, E.J., 1985. Relationship between petroleum composition and depositional environment of petroleum source rocks. AAPG Bull. 69, 1255–1268.
Morales, J.A., 2022. Tide Processes. In: Coastal Geology. Springer Textbooks in Earth Sciences, Geography and Environment. Springer, Cham, Switzerland, p. 477.
Morris, J.L., Leake, J.R., Stein, W.E., Berry, C.M., Marshall, J.E.A., Wellman, C.H., Milton, J.A., Hillier, S., Mannolini, F., Quirk, J., Beerling, D.J., 2015. Investigating Devonian trees as geo–engineers of past climates: linking palaeosols to palaeobotany and experimental geobiology. Palaeontology 58 (5), 787–801.
Omodeo-Sale, S., Deschamps, R., Michel, P., Chauveau, B., Suarez-Ruiz, I., 2017. The coal–bearing strata of the Lower Cretaceous Mannville Group (Western Canadian Sedimentary Basin, South Central Alberta), PART 2: factors controlling the composition of organic matter accumulations. Int. J. Coal Geol. 179, 219–241.
Panahi, A., Young, G.M., Rainbird, R.H., 2000. Behavior of major and trace elements (including REE) during Paleoproterozoic pedogenesis and diagenetic alteration of an Archean granite near Ville Marie, Quebec. Canada. Geochim. Cosmochim. Acta 64 (13), 2199–2220.
Potter, P.E., Shimp, N.F., Witters, J., 1963. Trace elements in marine and fresh-water argillaceous sediments. Geochim. Cosmochim. Acta 27 (6), 669–694.
Qian, K., Shi, H.X., 1982. Selection of medieval salinity measurement method in resource evaluation. Pet. Explor. Dev. 03, 32–38.
Qie, W., Liang, K., Königshof, P., 2019a. Devonian palaeoecosystems and palaeoenvironments of South China. Palaeobio. Palaeoenv. 99, 1–5.
Qie, W.K., Algeo, T.J., Luo, G., Herrmann, A., 2019b. Global events of the Late Paleozoic (Early Devonian to Middle Permian): a review. Palaeogeogr. Palaeoclimatol. Palaeoecol. 531, 109259.
Qie, W.K., Guo, W., Ma, X.P., Song, J.J., Xu, H.H., Qiao, L., Liang, K., Chen, B., Lu, J.F., Chang, J.Y., 2021a. Lithostratigraphuic subdivision and correlation of the Devonian in China. J. Stratigr. 45 (3), 286–302.
Qie, W.K., Sun, Y.L., Guo, W., Nie, T., Chen, B., Song, J.J., Liang, K., Yin, B.A., Han, S.P., Chang, J.Y., Wang, X.D., 2021b. Devonian–Carboniferous boundary in China. Palaeobio. Palaeoenv. 101, 589–611.
Ray, S., Chakraborty, T., 2002. Lower Gondwana fluvial succession of the Pench–Kanhan valley, India: stratigraphic architecture and depositional controls. Sediment. Geol. 151, 243–271.
Richardson, J.B., McGregor, D.C., 1986. Silurian and Devonian spore zones of the Old Red Sandstone Continent and adjacent regions. Bull. Geol. Surv. Can. 364, 1–79.
Rodríguez, W., Buatois, L.A., Mángano, M.G., Solórzano, E.J.M., Geology, P., 2018. Sedimentology, ichnology, and sequence stratigraphy of the Miocene Oficina Formation, Junín and Boyacá areas, Orinoco Oil Belt, Eastern Venezuela Basin. Mar. Pet. Geol. 92, 213–233.
Rong, J.Y., Chen, X., Su, Y.Z., Ni, Y.N., Zhan, R.B., Chen, T.E., Fu, L.P., Li, R.Y., Fan, J.X., 2003. Silurian palaeogeography of China. In: Landing, E., Johnson, M.E. (Eds.), Silurian Lands and Seas: Paleogeography outside of Laurentia, New York State Museum Bulletin, vol. 493, pp. 243–293.
Sageman, B.B., Murphy, A.E., Werne, J.P., Ver Straeten, C.A., Hollander, D.J., Lyons, T. W., 2003. A tale of shales: the relative roles of production, decomposition, and dilution in the accumulation of organic-rich strata, Middle–Upper Devonian, Appalachian Basin. Chem. Geol. 195, 229–273.
Saltzman, M.R., 2002. Carbon isotope ($\delta^{13}C$) stratigraphy across the Silurian–Devonian transition in North America: evidence for a perturbation of the global carbon cycle. Palaeogeogr. Palaeoclimatol. Palaeoecol. 187 (1–2), 83–100.
Sandberg, C.A., Ziegler, W., Dreesen, R., Butler, J.L., 1988. Late Frasnian mass extinction: conodont event stratigraphy, global changes, and possible causes. In: *Lunar and Planetary Inst., Global Catastrophes in Earth History: An Interdisciplinary Conference on Impacts, Volcanism, and Mass Mortality*.
Scotese, C.R., 2014. Atlas of Devonian Paleogeographic Maps, PALEOMAP Atlas for ArcGIS, volume 4, The Late Paleozoic, Maps 65–72, Mollweide Projection, PALEOMAP Project, Evanston, Ilinois, USA.
Shao, L.Y., Wen, H., Gao, X.Y., Spiro, B., Wang, X.T., Yan, Z.M., Large, D.J., 2022. Identification of Milankovitch cycles and calculation of net primary productivity of paleo-peatlands using geophysical logs of coal seams. Acta Geol. Sin. 96, 1830–1841.
Shen, W.C., Shao, L.G., Zhou, Q.Y., Liu, J.S., Eriksson, K.A., Kang, S.L., Steel, R.J., 2024. The role of fluvial and tidal currents on coal accumulation in a mixed-energy deltaic setting: Pinghu Formation, Xihu Depression, East China Sea Shelf Basin. Sedimentology 71, 173–206.
Shu, L.S., Yao, J.L., Wang, B., Faure, M., Charvet, J., Chen, Y., 2021. Neoproterozoic plate tectonic process and Phanerozoic geodynamic evolution of the South China Block. Earth-Sci. Rev. 216 (1).
Slattery, M.C., Gares, P.A., Phillips, J.D., 2006. Multiple modes of storm runoff generation in a North Carolina coastal plain watershed. Hydrol. Process. 20, 2953–2969.
Slavík, L., Hladil, J., 2020. Early Devonian (Lochkovian–early Emsian) bioevents and conodont response in the Prague Synform (CzechRepublic). Palaeogeogr. Palaeoclimatol. Palaeoecol. 549, 109148.
Slavík, L., Valenzuela-Ríos, J.I., Hladil, J., Chadimová, L., Liao, J.C., Hušková, A., Calvo, H., Hrstka, T., 2016. Warming or cooling in the Pragian? Sedimentary record and petrophysical logs across the Lochkovian–Pragian boundary in the Spanish Central Pyrenees. Palaeogeogr. Palaeoclimatol. Palaeoecol. 449, 300–320.
Steemans, P., 1989. Palynostratigraphie de l'Eodévonien dans l'ouest de l'Europe. In: Mémoires Explicatifs pour les Cartes Géologiques and Minéralogiques de la Belgique, vol. 27. Service Géologique de Belgique, Bruxelles.
Streel, M., 1967. Associations de spores du Dévonien Inférieur belge et leur signification stratigraphique. Ann. Soc. Geol. Belg. 90, 11–53.
Streel, M., Higgs, K., Loboziak, S., Riegel, W., Steemans, P., 1987. Spore stratigraphy and correlation with faunas and floras in the type marine Devonian of the Ardenne–Rhenish regions. Rev. Palaeobot. Palynol. 50, 211–229.
Syvitski, J.P.M., 1991. Principles, methods, and application of particle size analysis: principles and methods of geological particle size analysis. Cambridge Univ. Press 388, 3–21.
Tanavsuu-Milkeviciene, K.E., Plink-Bjorklund, P.E., 2009. Recognizing tide-dominated versus tide–influenced deltas: Middle Devonian strata of the Baltic Basin. J. Sediment. Res. 79, 887–905.
Taylor, A.M., Goldring, R., 1993. Description and analysis of bioturbation and ichnofabric. J. Geol. Soc. Lond. 150, 141–148.
Tissot, B.P., Welte, D.H., 1984. Petroleum Formation and Occurrence. Springer–Verlag, Berlin.
Tye, R.S., Coleman, J.M., 1989. Depositional processes and stratigraphy of fluvially dominated lacustrine deltas; Mississippi delta plain. J. Sediment. Petrol. 59, 973–996.
van Cappelle, M., Hampson, G.J., Johnson, H.D., 2018. Spatial and temporal evolution of coastal depositional systems and regional depositional process regimes: Campanian Western Interior Seaway, U.S.a. J. Sediment. Res. 88, 873–897.
Wadsworth, J., Boyd, R., Diessel, C., Leckie, D., Zaitlin, B.A., 2002. Stratigraphic style of coal and non–marine strata in a tectonically influenced intermediate accommodation setting: the Mannville Group of the Western Canadian Sedimentary Basin, south-Central Alberta. Bull. Can. Petrol. Geol. 50, 507–541.

Walker, C.T., 1968. Evaluation of boron as a paleosalinity indicator and its application to offshore prospects. AAPG Bull. 52 (5), 751–766.
Walker, C.T., Price, N.B., 1963. Departure curves for computing paleosalinity from boron in illites and shales. AAPG Bull. 47 (5), 833–841.
Wang, Y., 1994. Lower Devonian miospores from Gumu in the Wenshan District, Southeastern Yunnan. Acta Micropal. Sinica 11, 319–332.
Wang, Y.Y., Guo, W.Y., Zhang, G.D., 1979. Application of some geochemical indicators in determining of sedimentary environment of the Funing Group (Paleogene), Jin–Hu depression, Kiangsu Province. J. Tongji Univer. 02, 51–60.
Wang, W., Qin, Y., Liu, X., Zhao, J., Wang, J., Wu, G., Liu, J., 2011. Distribution, occurrence and enrichment causes of gallium in coals from the Jungar Coalfield, Inner Mongolia. Sci. China D Earth Sci. 54 (7), 1053–1068.
Wang, Y., Qie, W.K., Xu, H.H., Guo, W., Zhang, X.L., Lu, J.F., Huang, P., Wang, K., Peng, H.P., Chen, Y.X., Zhao, W.J., 2024. Subdivision and correlation of the Devonian clastic strata after the Kwangsian Orogeny in South China. J. Stratigr. 48 (2), 124–146.
Wei, W., Algeo, T.J., 2020. Elemental proxies for paleosalinity analysis of ancient shales and mudrocks. Geochim. Cosmochim. Acta 287, 341–366.
Weinerová, H., Bábek, O., Slavík, L., Vonhof, H., Joachimski, M.M., Hladil, J., 2020. Oxygen and carbon stable isotope records of the Lochkovian–Pragian boundary interval from the Prague Basin (Lower Devonian, Czech Republic). Palaeogeogr. Palaeoclimatol. Palaeoecol. 560, 110036.
Wu, H.R., 2001. Reinterpretation of the Kwangsi Orogeny. Chin. Sci. Bull. 45, 555–558.
Wu, Y., Gong, Y.M., Du, Y.S., 1997. Devonian Sequence Stratigraphy and Sea Level Change in South China. China University of Geosciences Press.
Xia, X.P., Nie, X.S., Lai, C.K., Wang, Y.J., Meffre, S., 2016. Where was the Ailaoshan Ocean and when did it open: a perspective based on detrital zircon U-Pb age and Hf isotope evidence. Gondwana Res. 36, 488–502.
Xue, J., Deng, Z., Huang, P., Huang, K., Benton, M.J., Cui, Y., Wang, D., Liu, J., Shen, B., Basinger, J.F., Hao, S., 2016. Belowground rhizomes in paleosols: the hidden half of an Early Devonian vascular plant. Proc. Natl. Acad. Sci. USA 113 (34), 9451–9456.
Xue, J.Z., Huang, P., Wang, D.M., Xiong, C.H., Liu, L., Basinger, J.F., 2018. Silurian Devonian terrestrial revolution in South China: taxonomy, diversity, and character evolution of vascular plants in a paleogeographically isolated, low-latitude region. Earth-Sci. Rev. 180, 92–125.
Xue, J.Z., Wang, J.S., Li, B.X., Huang, P., Liu, L., 2022. Origin and early evolution of land plants and the effects on Earth's environments. Earth Sci. 47 (10), 3648–3664.
Xue, J.Z., Li, B.X., Wang, J.S., Liu, L., Huang, P., Xiong, C.H., Shen, B., 2023a. Coupling relationship between radiation of early vascular plants and the long-term water cycle. Chin. Sci. Bull. 68, 1459–1472.
Xue, J., Wang, J., Huang, P., Liu, L., Huang, T., Zhang, L., Wang, X., Shen, B., Wang, D., Liu, J., Davies, N.S., Basinger, J.F., 2023b. The colonization of drylands by early vascular plants: evidence from Early Devonian fossil soils and in situ plant traces from South China. Earth-Sci. Rev. 237, 104290.
Ye, C., Yang, Y., Fang, X., Zhang, W., 2016. Late Eocene clay boron-derived paleosalinity in the Qaidam Basin and its implications for regional tectonics and climate. Sediment. Geol. 346, 49–59.
Yuri, Z.N., Eder, V.G., Zamirailova, A.G., 2008. Composition and formation environments of the Upper Jurassic–Lower Cretaceous black shale Bazhenov Formation (the central part of the West Siberian Basin). Mar. Pet. Geol. 25, 289–306.
Zhang, S.H., Liu, C.Y., Liang, H., Wang, J.Q., Bai, J.K., Yang, M.H., Liu, G.H., Huang, H. X., Guan, Y.Z., 2018. Paleoenvironmental conditions, organic matter accumulation, and unconventional hydrocarbon potential for the Permian Lucaogou Formation organic-rich rocks in Santanghu Basin. NW China. Int. J. Coal Geol. 185, 44–60.
Zhang, S.H., Xiao, L., Xue, J.Z., Meng, M.C., Qi, M., Cui, Y., Wang, D.M., 2021. Characteristics of stable carbon isotope of the Early Devonian plants from Yunnan Province and its palaeoclimatic significance. J. Paleaogeogr. 23 (5), 887–900.
Zhang, A.C., Lv, D.W., Zhang, Z.H., Raji, M., Gao, Y., Zhang, L.M., Wang, L.J., Du, W.X., Li, Z.K., 2024. Coal-derived rates of atmospheric dust deposition during the Jurassic-Cretaceous greenhouse periods. Gondwana Res. 125, 168–179.
Zhu, M., Wang, J.Q., Fan, J.H., 1994. Early Devonian fishes from Guijiatun and Xujiachong Formations of Qujing, Yunnan, and related biostratigraphic problems. Vertebr. Palasiat. 32, 1–20.